Improving High-Latitude Sea Surface Height Data Assimilation: Model-Based Vertical Covariance

ROBERT W. HELBER,[a] ELIZABETH M. DOUGLASS,[a] XIAOBIAO XU,[b] JULIE L. MCCLEAN,[c] ERIC P. CHASSIGNET,[b] ALAN J. WALLCRAFT,[b] AND ALEXANDRA BOZEC[b]

[a] *Naval Research Laboratory, Stennis Space Center, Hancock County, Mississippi*
[b] *Center for Ocean-Atmospheric Prediction Studies, Florida State University, Tallahassee, Florida*
[c] *Scripps Institution of Oceanography, University of California San Diego, La Jolla, California*

(Manuscript received 12 February 2025, in final form 9 March 2026, accepted 25 March 2026)

ABSTRACT: The most important source of information constraining the Navy's operational global ocean forecasting system is the sea surface height anomaly (SSHA) as measured by satellite altimetry. These surface observations inform a one-dimensional (1D) variational analysis to create synthetic profiles of temperature and salinity, which approximate the subsurface ocean structure associated with the observed SSHA that is assimilated in a three-dimensional variational analysis. The 1D analysis requires vertical error covariances that relate the differences in values between temperature and salinity at different depths. These vertical covariances are computed empirically from historical in situ observation profiles of temperature and salinity. The approach ensures that the assimilated profiles have realistic structure without drifting. A shortcoming of this approach is the availability of in situ observations extending at least 1000 m deep. Observations are sparser at high latitudes, often do not include salinity, and reach relatively shallow depths. We wish to use model data to address these limitations. Here, we show that using a global 30-yr model run to compute vertical covariances solves sampling issues while continuing to maintain accuracy. While the covariances derived from the model generally compare well with the observed ones, in some areas of the ocean, the numerical ocean model has different vertical covariances. A new method for determining where synthetics are most valuable is presented. The implication of having model-derived covariances is the ability to extend covariance information at high latitude where in situ observations are sparse or have sampling anomalies. Results also suggest that salinity, if observed, would provide substantial improvement to the system.

SIGNIFICANCE STATEMENT: The purpose of this study is to understand present high northern latitude ocean numerical forecasting capabilities and shortcomings related to the use of sea surface height measurements derived from satellite, which are used to correct ocean forecast models that diverge from reality due to chaos. This is important because changing conditions are amplified at high latitudes and require modifications to present forecasting systems. Ocean forecasting is challenging in these regions due to few in situ observations and unique oceanographic conditions. Our paper describes new methods in data-poor regions and more accurate model uncertainty estimates for maximizing forecast capabilities.

KEYWORDS: Arctic; Mesoscale processes; Ocean dynamics; Climatology; Data assimilation; Ocean models

1. Introduction

The most important source of observational information used to constrain mesoscale variability in operational, data assimilative, ocean forecasting systems is the sea surface height anomaly (SSHA) as measured by satellite altimetry. SSHA data are typically assimilated using empirically derived covariances (Miyazawa et al. 2009) and ensemble optimal interpolation methods (Oke et al. 2008) that modify the interior physical variables (temperature, salinity, velocities) so that their temperature and salinity profile anomalies give rise to a steric SSHA that matches the observed SSHA. The method used by the U.S. Navy differs in the sense that the operational implementation of SSHA data assimilation employs a one-dimensional (1D) variational approach to create "synthetic" ocean profiles of temperature and salinity (Helber et al. 2013) that are then assimilated in a three-dimensional variational data assimilation (3DVAR) system (Metzger et al. 2014). The term synthetic is used to describe a vertical ocean profile constructed from only surface observations as described in section 2 and the appendix. These synthetic profiles approximate the subsurface ocean structure associated with the observed SSHA, sea surface temperature, and input mixed layer depth. The advantage of this approach for assimilated SSHA data are the constraints to the climatological mean and vertical structure. The synthetics are created as anomalies from climatology and thus maintain realistic structure that will not drift. While this system for assimilation of SSHA data into ocean models works well for most of the ocean (Thoppil et al. 2021), it may not be optimal for the Arctic and subarctic seas because the climatological information is less reliable due to poor data sampling and rapidly changing conditions. To understand how these limitations impact the success of the assimilation scheme, this paper describes research for improving high-latitude SSHA data assimilation in ocean forecasting of the Arctic and subarctic seas, northward of 40°N. The end goal of this research is to

Corresponding author: Robert W. Helber, robert.w.helber.civ@us.navy.mil

DOI: 10.1175/JTECH-D-25-0014.1

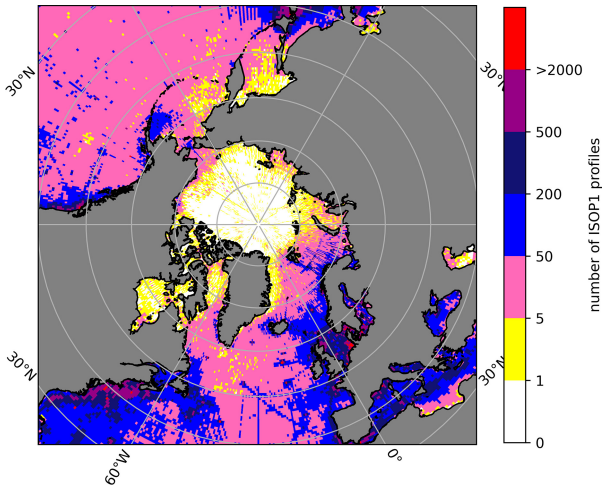

FIG. 1. The number of in situ observations in 1/2° squares in the ocean. The data numbers shown are from the database used to create ISOP1.

create accurate, data assimilative ocean forecasts for the Arctic and subarctic seas.

At the core of the Navy's SSHA data assimilation approach is empirical vertical covariance information derived from historical in situ observational temperature and salinity profiles from the Navy's Master Oceanographic Observation Dataset (MOODS) (Bauer 1985; Teague et al. 1987). The covariances are essential in the 1D variational methods for creating the synthetics. The observed in situ profiles, composed of conductivity–temperature–depth (CTD), expendable bathythermographs (XBTs), and mooring glider profiles, and other data from profiling observation systems provide relatively high-vertical-resolution profiles at a coarse nonuniform, horizontal and temporal sampling coverage. Figure 1 shows the number of profiles, in 1/2° bins, used in the Navy's Improved Synthetic Ocean Profile system, version 1 (ISOP1) (Helber et al. 2013). Many of the observations occur where research vessels have sailed, but many of the observations occur randomly as sampled by the Argo autonomous vertical-profiling float program. There are many more profiles near the coasts in the Northern Hemisphere. Also, the sampling is nonuniform, and in the vertical, the number of observations decreases with depth. The result is a dataset that resolves the mesoscale vertical structure over most of the ocean that we use to create vertical correlation estimates in monthly climatological averages. However, at high latitude, these observations have a pattern that decreases in number toward the north pole, making it hard to resolve the mesoscale vertical structure in the Arctic and subarctic seas. Furthermore, sea surface height data assimilation at high latitude is severely limited by the available satellite SSHA observations which are unavailable northward of approximately 75°N. In addition, the Navy operational system currently turns off synthetic profiles derived from SSHA if the vertical ocean thermal stratification is small (Douglass et al. 2026, unpublished manuscript) (Fig. 2). This was implemented because of the perception that these profiles were unreliable under this condition. In Fig. 2, the white areas have ice coverage for 31 December 2017, and thus, areas where synthetics are created are ice free. A key goal of this research is to extend SSHA data assimilation into the areas that are presently neglected, as shown in Fig. 2a.

The current Navy approach relies on historical observations, but given the latest advancement in ocean modeling, one can envision that the mesoscale vertical error covariances could be derived from multidecadal high-resolution global ocean models (Chassignet et al. 2020) if the models have been shown to be representative of the observed variability. In this

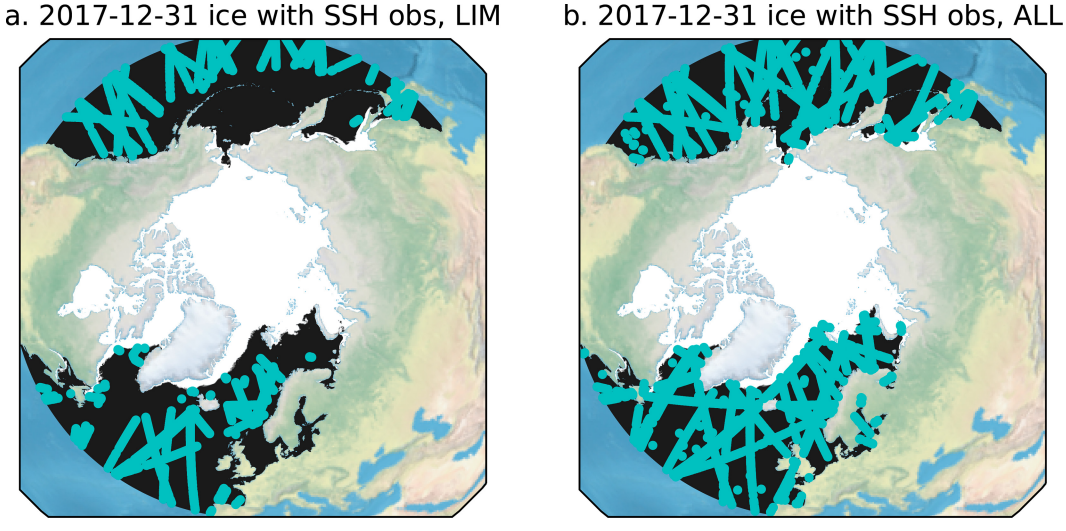

FIG. 2. The locations of synthetic profiles (cyan dots) and the ice coverage (white ocean areas) on 31 Dec 2017. (left) The synthetic profiles are restricted because of low stratification, where the difference in temperature between 1000 and the surface is less than 3°C. (right) The synthetic profiles are not restricted and are produced further northward.

paper, we explore the option of replacing the in situ observations, in the calculation of the ISOP vertical error covariances, with global ocean modeling high-resolution 1/12° data created using the Hybrid Coordinate Ocean Model (HYCOM) (Bleck 2002; Chassignet et al. 2003) over the 1958–2022 time period (Chassignet et al. 2020). The advantage of this approach is that the model has uniform coverage of the global ocean in space and time, including at high latitude where in situ observations are sparse. Thus, at high latitude, we will have significantly more model output than in situ observations. A potential drawback, however, is that the model results may not accurately represent all the variability that occurs in the ocean, due to its limited horizontal resolution, approximate parameterizations, missing physics, inaccurate bathymetry, and forcing, etc.

In section 2, we describe the methods used for creating ISOP1 synthetic ocean profiles from inputs of SSHA, sea surface temperature, and mixed layer depth. The methods for computing vertical covariances and the correlation length scales, extracting model data for five sampling fidelity test cases, and validating the results relative to observational profiles are also discussed in section 2. Section 3 describes the validation, relative to independent in situ observations, of the new model-formulated synthetics compared to traditional observation-based methods. Also, in section 3, we describe the observing system simulation experiment (OSSE) for the Arctic and subarctic seas also described by Douglass et al. (2026, unpublished manuscript) (see also Fine et al. 2023) that utilizes the new model-based synthetics. We discuss the practical application of this system at high latitudes and in regions of the ocean where the HYCOM model data may provide the greatest advantages over insufficient in situ observations. Finally, we explore veracity of the synthetics relative to the temperature and salinity properties over the water column and suggest a new method for determining when synthetics are most accurate and find that the lack of salinity input is particularly detrimental. Section 4 contains a summary and conclusions for this research.

2. Methods

a. Synthetic profile methods

The system for constructing synthetic profiles from surface observations uses real-time inputs of sea surface temperature (SST), $\tilde{T}_1$, and height anomaly, $\delta\tilde{h}$, and an estimate of the surface mixed layer depth (MLD). The cost function, to create one synthetic profile at a location, is given by

$$\begin{aligned} J = {} & \delta\mathbf{x}^{(\mathrm{clim})\mathrm{T}}\mathbf{B}^{-1}\delta\mathbf{x}^{(\mathrm{clim})} + \delta\mathbf{d}^{(\mathrm{clim})\mathrm{T}}\mathbf{B}^{(d)-1}\delta\mathbf{d}^{(\mathrm{clim})} \\ & + \delta\mathbf{x}^{(\mathrm{eof})\mathrm{T}}\mathbf{V}^{-1}\delta\mathbf{x}^{(\mathrm{eof})} + \delta\mathbf{d}^{(\mathrm{eof})\mathrm{T}}\mathbf{V}^{(d)-1}\delta\mathbf{d}^{(\mathrm{eof})} \\ & + \delta\tilde{T}_1^{(\mathrm{obs})}R^{(\mathrm{SST})-1}\delta\tilde{T}_1^{(\mathrm{obs})} + [\mathbf{L}\delta\mathbf{x}^{(\mathrm{clim})} - \delta\tilde{h}^{(\mathrm{clim})}] \\ & \times R^{(\mathrm{SSHA})-1}[\mathbf{L}\delta\mathbf{x}^{(\mathrm{clim})} - \delta\tilde{h}^{(\mathrm{clim})}]. \end{aligned} \tag{1}$$

The first two terms on the right-hand side of Eq. (1) contain the deviation of the solution from climatology, $\delta\mathbf{x}^{(\mathrm{clim})}$, and the deviation of the vertical gradient of the solution from that of climatology, $\delta\mathbf{d}^{(\mathrm{clim})}$. The background error covariance and the background vertical gradient error covariance are $\mathbf{B}^{-1}$ and $\mathbf{B}^{(d)-1}$, respectively. The next two terms are the deviation of the reduced empirical orthogonal function (EOF) mode, solution from climatology, $\delta\mathbf{x}^{(\mathrm{eof})}$, and the deviation of the reduced EOF mode, vertical gradient of the solution from that of climatology, $\delta\mathbf{d}^{(\mathrm{eof})}$. The diagonal matrix of variances and the vertical gradient diagonal matrix of variances are $\mathbf{V}^{-1}$ and $\mathbf{V}^{(d)-1}$, respectively. The last two terms on the right-hand side of Eq. (1) contain the deviation of observed SST from the solution, $\delta\tilde{T}_1^{(\mathrm{obs})}$, the deviation of observed SSHA from the climatology, $\delta\tilde{h}^{(\mathrm{clim})}$, and the deviation of climatological SSHA from the solution, $\mathbf{L}\delta\mathbf{x}^{(\mathrm{clim})}$, where $\mathbf{L}$ is a linear operator that computes steric height. The diagonal matrix of SST error variance and the diagonal matrix of SSHA error variance are $R^{(\mathrm{SST})}$ and $R^{(\mathrm{SSHA})}$, respectively. Equation (1) and these variables are described in more detail in the appendix.

A key component of this one-dimensional variation analysis is the vertical covariance model derived from empirical in situ observations, which resolve the mesoscale vertical structure over most of the ocean. The vertical covariances enable the minimization of Eq. (1) to project the surface information downward into the ocean to create a synthetic profile that is statistically consistent with the mesoscale vertical structure. In some regions of the ocean, such as the Arctic and subarctic seas, in situ observations are not plentiful enough to provide adequate vertical covariances. Thus, in this research, we investigate the feasibility of using global model data to create vertical covariance data.

The vertical covariances are split into correlations and variances such that

$$\mathbf{B} = \mathbf{UCU}, \tag{2}$$

where the monthly climatological standard deviation is $\mathbf{U}$ and monthly climatological correlation is $\mathbf{C}$.

A key component of making synthetics is the structure of the vertical covariances $\mathbf{B}$ and $\mathbf{B}^{(d)}$. Each of those has both variances and correlations. An example of correlations from a high-latitude location (70°N, 3°E), for the month of June, is shown in Fig. 3, and the climatological standard deviation is shown in Fig. 4. Figures 3 and 4 are for the summer month of June when, at high latitude, in situ observations are more plentiful. The data used to construct these covariances are from the original ISOP1 data shown in Fig. 1. At this location, the correlations were computed from 294 in situ profiles observations within a 2° search radius. The data for the correlation are weighted by the distance from the analysis location.

The autocorrelations in Figs. 3c and 3b have diagonal elements that are nearly one, but not exactly one, because the correlations are constructed from six EOF modes, for reduction in data storage. The cross correlations for salinity S with potential temperature T (Fig. 3d) and T with S (Fig. 3a) are transposes of each other. The depth of the climatological mixed layer for June can be seen most clearly in the salinity autocorrelation (Fig. 3b), where the mixed layer is negatively correlated with the deep ocean, in the Lofoten Basin at 70°N, 3°E (Raj et al. 2020). The vertical gradient correlations (see the appendix; Fig. A1) have substantially different structures

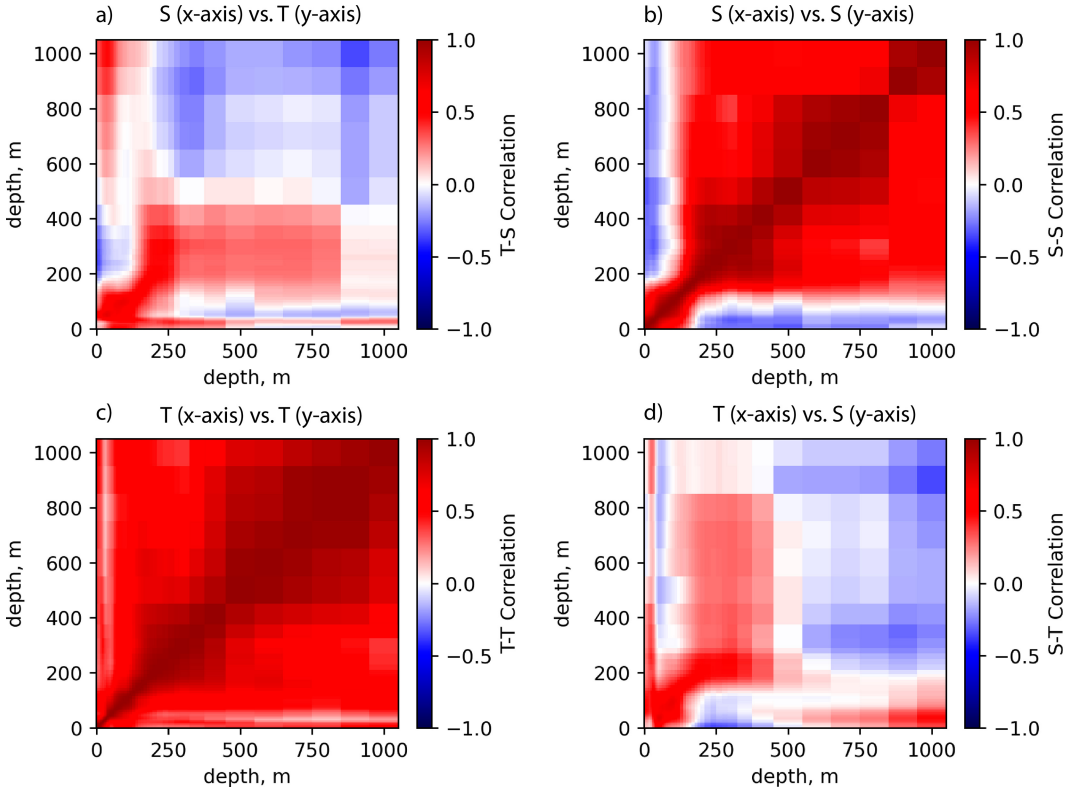

FIG. 3. The vertical correlations for T and S at 70°N, 3°E for June. (b),(c) The autocorrelations for T and S are along the diagonal. (a),(d) The off-diagonal cross correlations for S with T and T with S. Since the correlations go from 0 to 1000 m, the x and y axes cover the same depths. The block structure indicates there are 47 depth levels in the upper 1000 m, where the block indicates depth bins that get larger as depth increases. At this location, the correlations were computed from 294 in situ profile observations.

that represent persistent gradients and inflection points, on average, found in the historical profiles.

As shown in Eq. (2), the covariance is the correlation multiplied by the diagonal variance, **U**, which contains both the T and S variances along the diagonal (see the appendix). The square root of the variance (standard deviation), for T and S, at the location 70°N, 3°E, in the Lofoten Basin of the Norwegian Sea, is shown in Fig. 4. One characteristic of this location in the ocean is that the largest standard deviation occurs at the surface, as compared to the midlatitude ocean where the largest variance occurs in the thermocline (Helber et al. 2023).

The covariances are constructed from MOODS data for each month at every 1/2° location in the ocean. To help visualize the spatial variability of the correlations, we integrate the correlation at depth level k with all the other depths, thereby

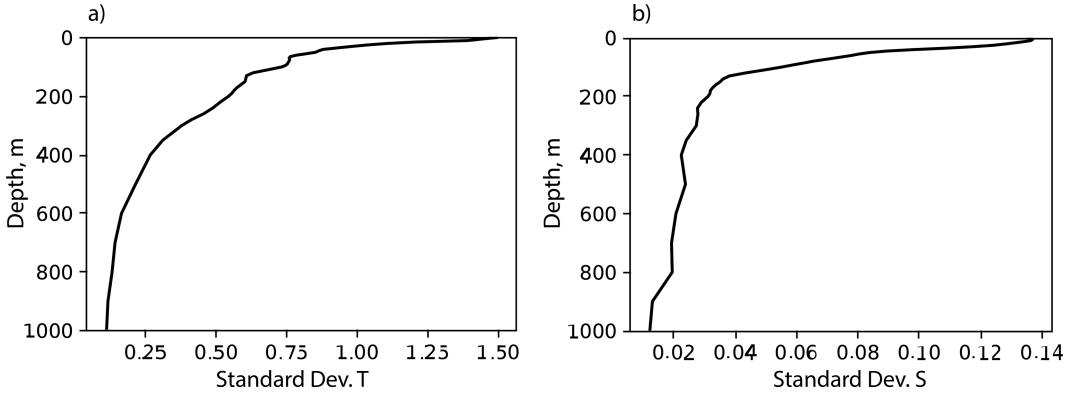

FIG. 4. The standard deviation profile for T and S for June at 70°N, 3°E, corresponding with the correlations shown in Fig. 3.

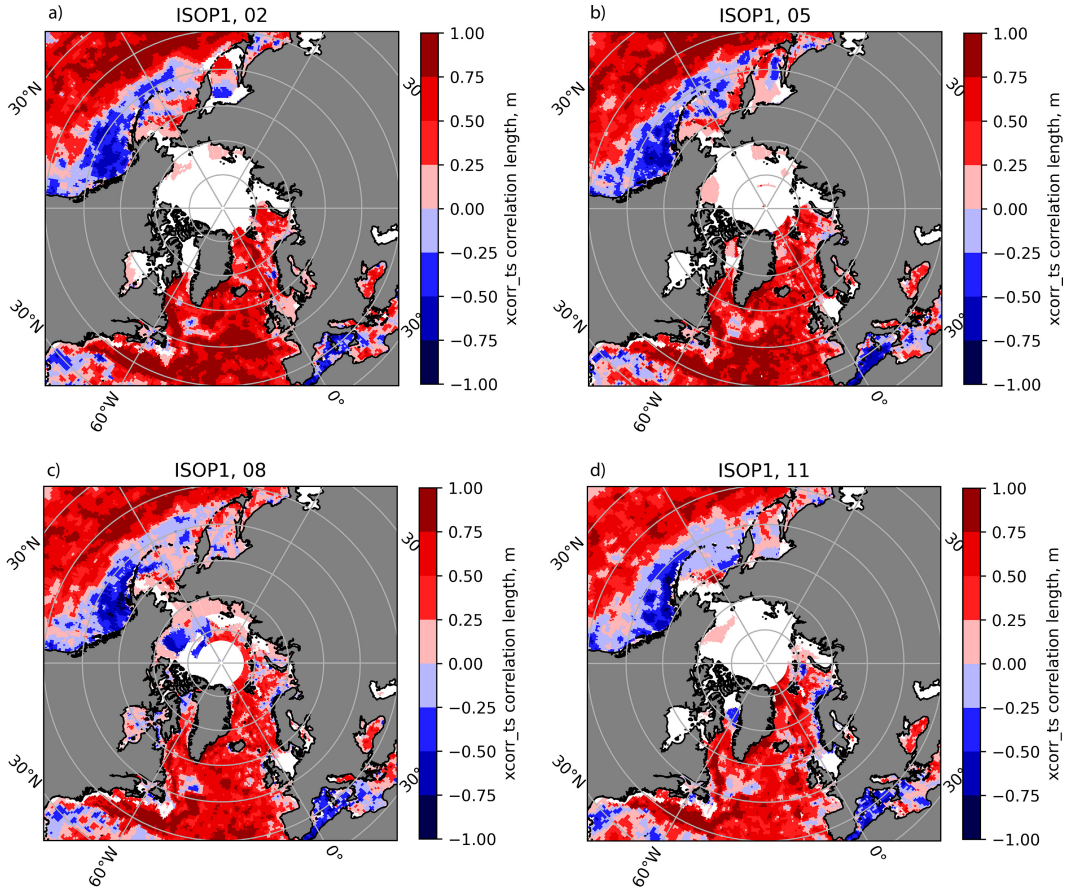

FIG. 5. Depth average cross correlation for T and S at each grid point, computed from the ISOP1 dataset, for the months of (a) February, (b) May, (c) August, and (d) November. White areas have no cross correlation computed due to lack of data.

providing a single number to represent the nature of the correlation at each grid point. For each of the correlation components in Eq. (2), we compute

$$\overline{C}_k = \frac{\sum_{i=1}^{\mathrm{nz}} C_{ik}|z_i - z_k|}{\sum_{i=1}^{\mathrm{nz}} |z_i - z_k|}, \tag{3}$$

where C_{ik} is the correlation between depth level i and k, where $i \neq k$, and nz is the total number of depth levels. Thus, $\overline{C}_k$ is the depth-weighted average correlation relative to depth level k. To obtain a characteristic correlation over the full water column down to 1000 m, we compute a depth average correlation such that

$$\langle C \rangle = \sum_{k=1}^{\mathrm{nz}} \overline{C}_k. \tag{4}$$

If every depth level were perfectly correlated with each other depth, then the correlation $\langle C \rangle = 1$.

To show the spatial variability of the average T versus S cross correlation, we plot the vertically averaged correlation [Eq. (4)] at each grid point for the months of February, May, August, and November (Fig. 5). Notice that there is modest seasonality in the vertically averaged correlation, computed from the ISOP1 dataset. During the rest of the year, there is not enough data (<15 observations at each depth) in the Arctic to compute vertical correlations. The blue areas indicate that much of the T versus S cross correlations with depth are negative, such as in the Gulf of Alaska. In the next section, we will describe additional sets of data sources and sampling strategies that allow us to demonstrate the effectiveness of model based covariances and the role of shifting climate.

b. *Data sampling strategies*

For ISOP1, the fidelity of the MOODS observations was determined from the available data collected at random locations around the global ocean up until the calendar year 2008. Using HYCOM model data, however, we are not restricted to the location of the in situ observations. The model output for the full grid domain covers years from 1964 through 2022. To evaluate the impact of spatial sampling, we extract the model data in three different levels of fidelity. The "obs-obs" fidelity is to extract the model data at the ISOP1 observation

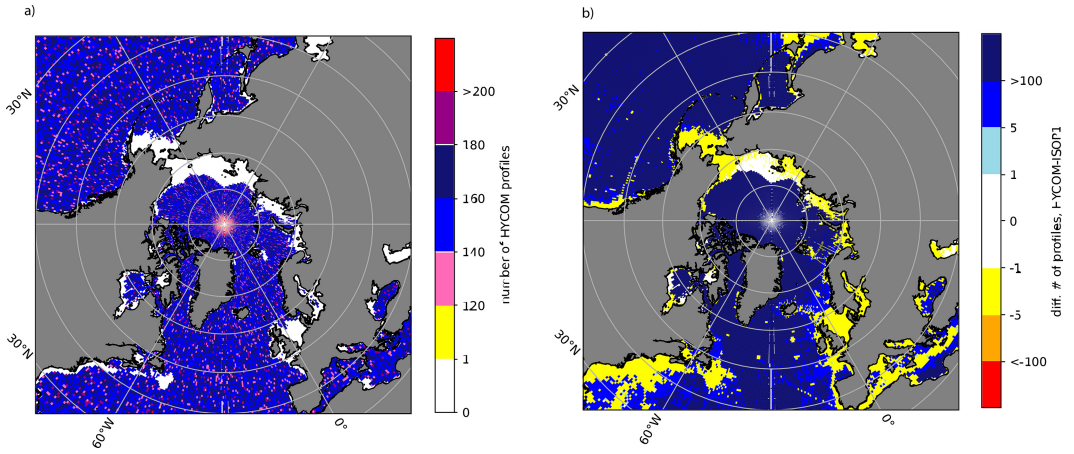

FIG. 6. The number of in situ observations in 1/2° squares in the ocean. (a) The data numbers are from the HYCOM data for 10% of the 0.5° bin selection (see text and Table 1). (b) The numbers are for the difference in the number of profiles for HYCOM-05deg minus ISOP1.

locations and at the observation depths. Since the model has full water column coverage over the global ocean, we also extract full water depth model data at the observation locations (called "obs-full"). The horizontal distribution of these data is the same as that for ISOP1 in Fig. 1. Then, to take advantage of the higher fidelity of the model data, we extract model data at 1/2° resolution, globally every 10 days for 36 samples a year (called "05deg"). The result of this selection was too much data for our analysis programs. For this reason, we randomly in time subsampled these data keeping 10% of the total number of profiles. This approach results in a dataset with roughly 200 profiles per 1/2° bin. Thus, this 10% randomly subsampled dataset has a uniform distribution of profiles globally (Fig. 6). Near the coast, however, there are more profiles in the in situ–observed dataset, as can be seen in the yellow areas of difference between the "05deg" minus the ISOP1 "obs" sampling in Fig. 6b. The sampling strategy for the model-based covariances HYCOM-obs-obs and HYCOM-obs-full used data for the period from 1964 through 2008 to match the ISOP1 in situ observation period. The case HYCOM-05deg data period was from 1964 to 2016. To evaluate longer-term shifts in the ocean's covariance state, we include a test case HYCOM-last-decade, which used data from 2013 through 2022. Because of the shorter time length, we increased the percentage to 20% of the initial 10-day sampling rate. There is a new version of ISOP2 that has newer observations with the distribution shown in Fig. 7. Overall, there is an increase in the number of profiles, with a modest increase in the Arctic. The list of data fidelity and sampling strategy is shown in Table 1.

To see the effect of the sampling strategy on the correlations, we plot the average cross correlation [Eq. (4)] for the ISOP1, ISOP2, HYCOM-obs-obs, and HYCOM-05deg test cases in Fig. 8. The correlations for May are shown representing

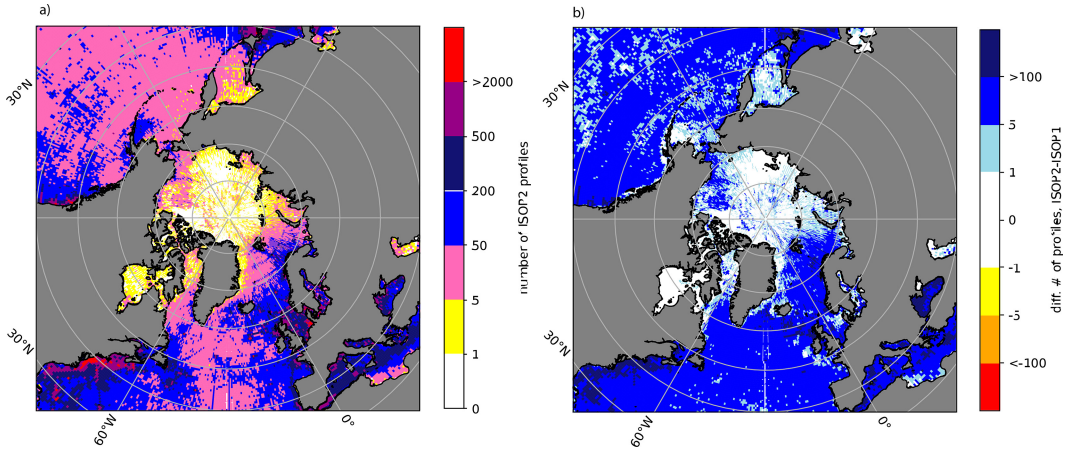

FIG. 7. The number of in situ observations in 1/2° squares in the ocean. (a) The data numbers are from the database used to create the ISOP system version 2. (b) The numbers are for the difference in the number of profiles for ISOP2 minus ISOP1.

TABLE 1. List of covariance dataset features.

Label	Source	Date range	Depths	Fidelity location
ISOP1	OBS	<1920–2008	OBS	OBS (ISOP 1)
ISOP2	OBS	<1920–2019	OBS	OBS (ISOP 2.1)
HYCOM-obs-obs	HYCOM	1964–2008	OBS	OBS (ISOP 1)
HYCOM-obs-full	HYCOM	1964–2008	MODEL	OBS (ISOP 1)
HYCOM-05deg	HYCOM	1964–2016	MODEL	10% of 0.5° selection
HYCOM-last-decade	HYCOM	2013–22	MODEL	20% of 0.5° selection

a transition month between the spring and summer when ocean sampling tends to be greater than winter months at high latitude. Winter months have less data coverage in the Arctic. We see that the ISOP1 sampling strategy has the fewest valid correlation values in the Arctic Ocean. To make valid *T*/*S* cross correlations, observations must have good values over the entire depth range to 1000 m. In the Arctic, HYCOM is more reliable in this way. The original ISOP1 data were limited in the Arctic (Fig. 8a). The ISOP2 sampling strategy has good coverage in the Arctic, and the HYCOM-05deg case has the greatest coverage. In the central Arctic, HYCOM-05deg shows a positive *T*/*S* cross correlation, whereas the ISOP2 data have a negative cross correlation. This also occurs in Baffin Bay, where the HYCOM-obs-obs and the HYCOM-05deg both have negative cross correlations, whereas ISOP1 has positive. In these regions, the HYCOM-05deg derived solution has the opposite sign compared to the observed data, apparently due to the higher sampling strategy.

3. Synthetic profile validation

a. Test cases

The goal of this analysis is to evaluate synthetics created using numerical ocean model forecast data and vertical error

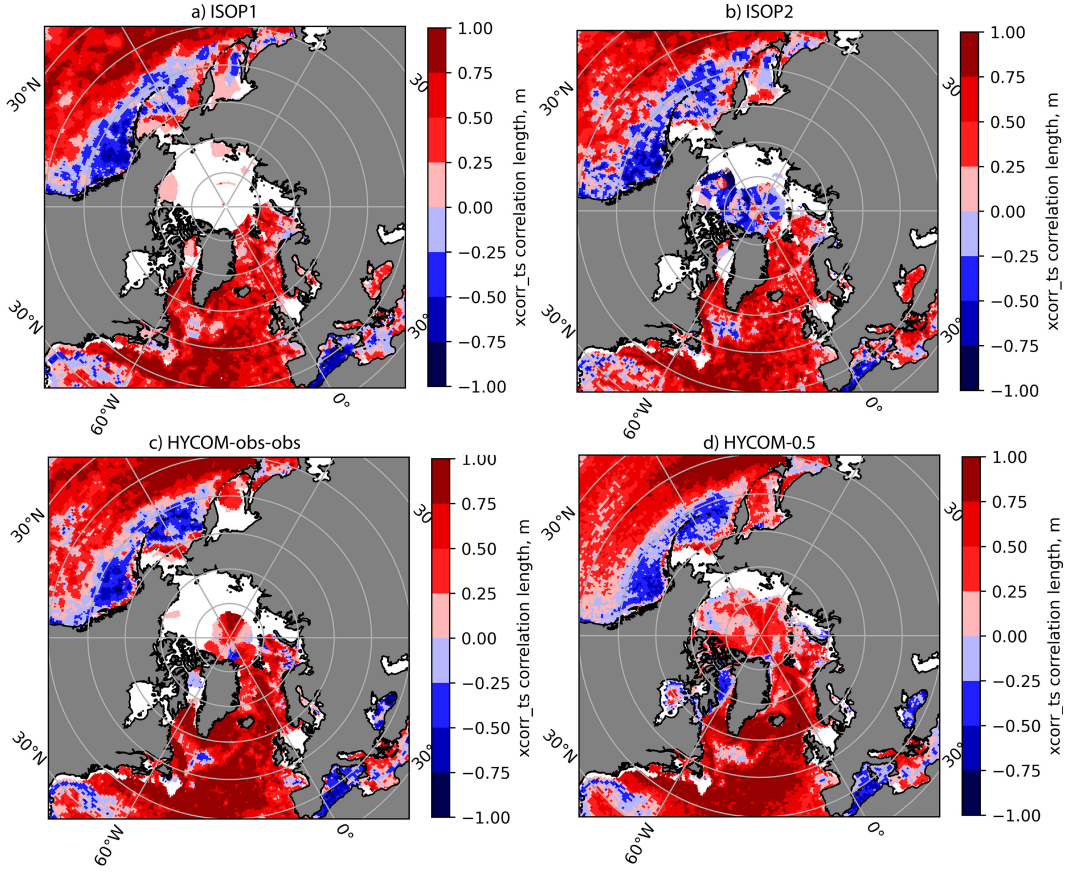

FIG. 8. The temperature vs salinity cross correlation for (a) ISOP1, (b) ISOP2, (c) HYCOM-obs-obs, and (d) HYCOM-05deg at each 1/2° grid point for the Arctic Ocean and the subpolar seas for May. White areas have no cross correlation computed due to lack of data.

TABLE 2. Synthetic vs MOODS validation cases including the source of steric height (STHT), monthly and annual average, and the background vertical covariances.

Case name	SST source	STHT monthly	STHT annual	STHT	SSHA	Vertical covariance
	$T_1^{(\mathrm{obs})}$	$h^{(\mathrm{clim})}$	$h^{(\mathrm{annual4})}$	$\tilde{h}$	$\delta\tilde{h}$	**B = UCU**
ISOP1	OBS SST	ISOP1 data	GDEM4 annual STHT	OBS T/S profile	$\tilde{h} - h^{(\mathrm{annual4})}$	ISOP1 data
ISOP2	OBS SST	ISOP2 data	GDEM4 annual STHT	OBS T/S profile	$\tilde{h} - h^{(\mathrm{annual4})}$	ISOP2 data
HYCOM-OBS-OBS	OBS SST	HYCOM-OBS-OBS data	GDEM4 annual STHT	OBS T/S profile	$\tilde{h} - h^{(\mathrm{annual4})}$	HYCOM-OBS-OBS data
HYCOM-OBS-FULL	OBS SST	HYCOM-OBS-FULL data	GDEM4 annual STHT	OBS T/S profile	$\tilde{h} - h^{(\mathrm{annual4})}$	HYCOM-OBS-FULL data
HYCOM 05deg	OBS SST	HYCOM 05deg data	GDEM4 annual STHT	OBS T/S profile	$\tilde{h} - h^{(\mathrm{annual4})}$	HYCOM 05deg data
HYCOM 05deg L-DEC	OBS SST	HYCOM 05deg last decade data	GDEM4 annual STHT	OBS T/S profile	$\tilde{h} - h^{(\mathrm{annual4})}$	HYCOM 05deg last decade data

covariances (see Table 1) for sea surface height (SSH) data assimilation in a cycling system. To evaluate the quality of synthetic profiles themselves, outside of the data assimilation system, we use a method for creating synthetics to match actual observed in situ profiles. To do this, we create synthetic profiles using inputs from MOODS observed in situ profiles that are not included in creation of the covariances. The MOODS profiles we use, for the years 2019, 2020, and 2021, are independent from the data used to create the covariances. The inputs for SST, MLD, and SSHA used to create the synthetics come from the MOODS T and S profiles for each case listed in Table 1. SST is taken from the shallowest T in the profile, and the MLD and SSHA are computed from the observed profile. All profiles selected for this purpose have both T and S, have a value at least 12 m from the surface, and extend to at least 1000 m. Thus, for each observed profile, we have a matching synthetic for each case. These synthetics represent the best possible representation of the profiles that the system can create, since the inputs come directly from the profiles themselves. The annual-mean steric height (see the appendix) comes from the Navy's Generalized Digital Environmental Model (GDEM), version 4 (GDEM4), ocean

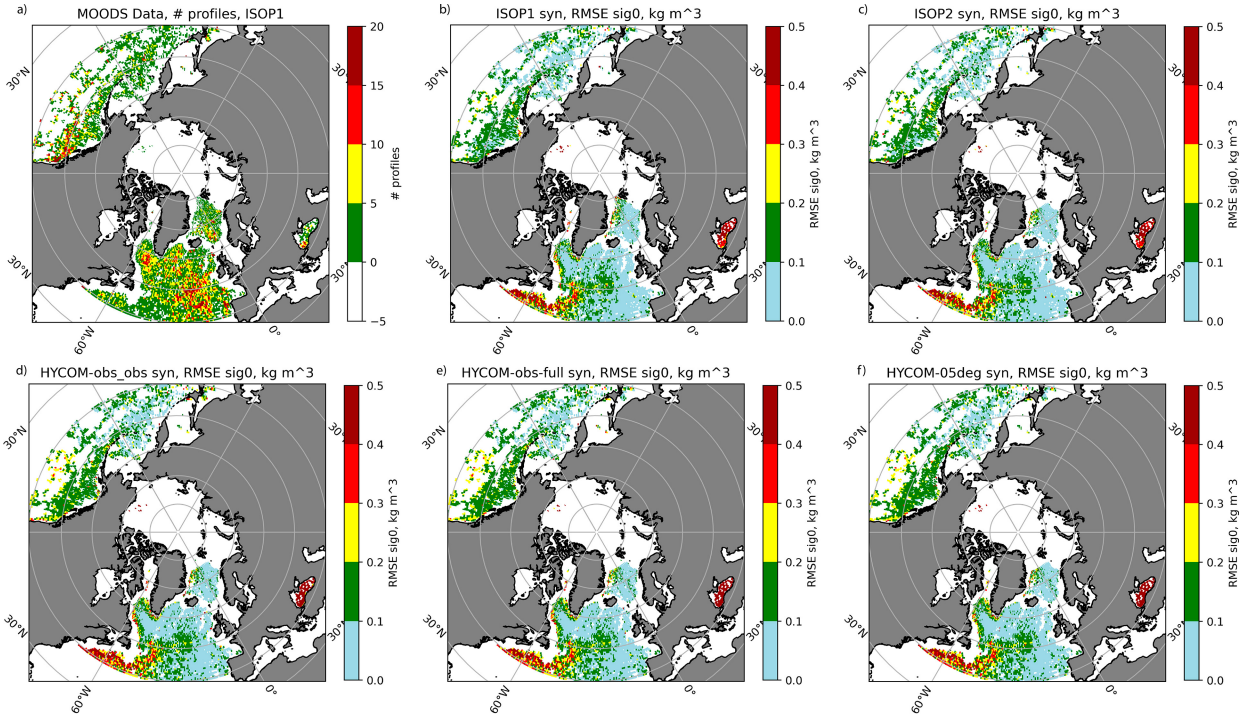

FIG. 9. The synthetic-mean RMSE for σ_0 relative to the MOODS in situ profile observations, for years 2019, 2020, and 2021, in 1° latitude and longitude bins. (a) The number of observations in each bin. The synthetic test cases are (b) ISOP1, (c) ISOP2, (d) HYCOM-obs-obs, (e) HYCOM-obs-full, and (f) HYCOM-05deg, as listed in Table 2.

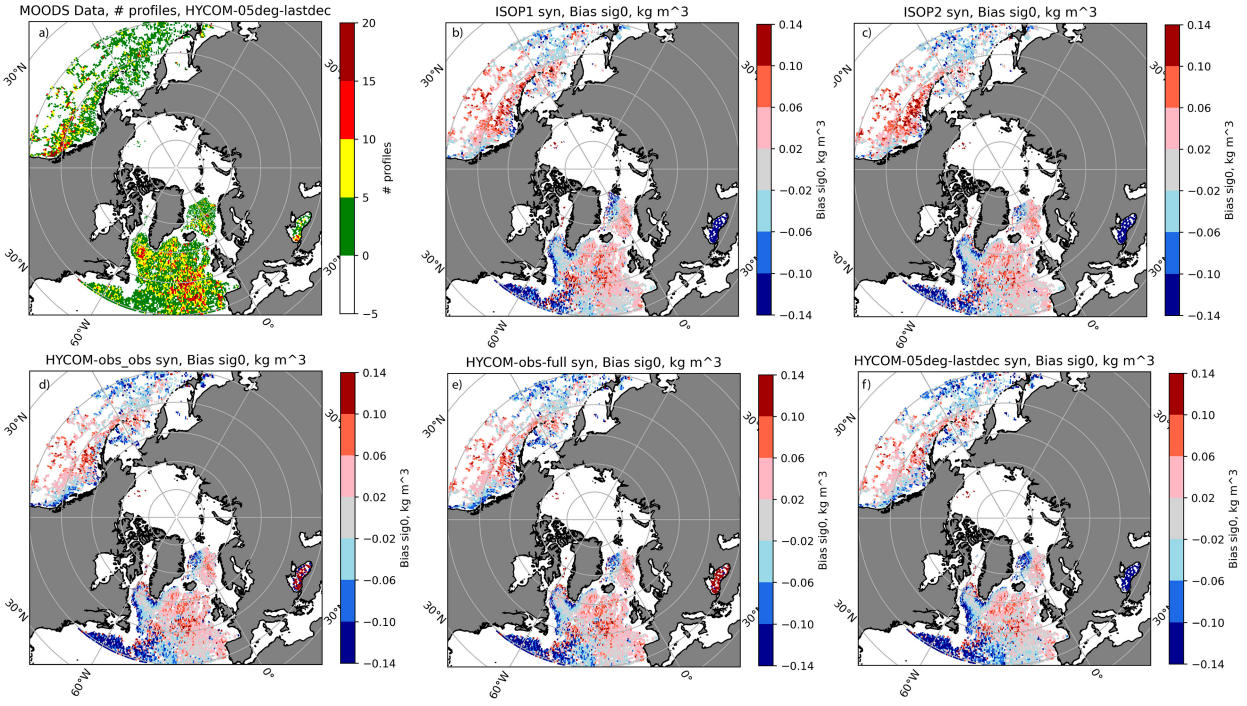

FIG. 10. The synthetic-mean BIAS for σ_0 relative to the MOODS in situ profile observations, for years 2019, 2020, and 2021, in 1° latitude and longitude bins. (a) The number of observations in each bin, which are identical to those in Fig. 9a. The synthetic test cases are (b) ISOP1, (c) ISOP2, (d) HYCOM-obs-obs, (e) HYCOM-obs-full, and (f) HYCOM-05deg-lastdec, as listed in Table 2.

climatology, (Carnes et al. 2010). The synthetic validation cases are listed in Table 2.

The only difference between each of the test cases is the vertical error covariance data used to make the synthetics and the internal reference monthly steric height [STHT monthly; $h^{(\mathrm{clim})}$] as described above and in the appendix. Part of the calculation of the monthly vertical error covariance is the monthly mean and variance of the data used to create the correlations. As explained in the appendix, there is also a term in Eq. (A17) that involves the monthly mean steric height, $h^{(\mathrm{clim})}$, which is computed from the same data used to make the covariances. The annual-mean steric height, however, is computed from the GDEM, version 4, ocean climatology of T and S. Thus, there is a difference in the origin of the climatological mean versus the annual-mean steric height for all cases except for the ISOP1 test case. In the case of ISOP1, the annual and monthly climatological-mean steric height is computed from the same data. In all other cases, these two quantities are slightly different. This difference is minor since the monthly climatological-mean anomaly is separate from the annual-mean anomaly. The system equates the consistent anomalies, not the total steric height. The synthetic steric height anomaly is equated with the satellite SSH anomaly. This inconsistency is likely negligible because HYCOM is initialized from the same GDEM version as is used for the mean steric height. Though small, the difference between a HYCOM versus in situ–derived steric height could give the HYCOM test cases slightly larger errors.

To summarize the errors, we compute σ_0 (surface referenced potential density) root-mean-square error (RMSE) over depth for each profile, binned in 1° boxes northward of 40°N (Fig. 9). The number of observations, for the years 2019, 2020, and 2021, in each box is shown in Fig. 9a. In the test cases where the covariances are derived from in situ observations, ISOP1 and ISOP2 test cases (Figs. 9b,c), there are more low RMSE values less than 0.1 kg m^{-3}(light blue boxes) in the Gulf of Alaska and Bering Sea. This indicates ISOP1 and ISOP2 have smaller RMSE values compared to the HYCOM data cases, in these areas. The RMSE values are comparable in the Atlantic Ocean, Irminger Basin, and the Greenland Sea, in all test cases. Unfortunately, there are few independent validation profiles in the Arctic Ocean and the Baffin Bay. Thus, these two regions cannot be evaluated for veracity.

Looking at the synthetic profile bias (convention is synthetic–observation) in σ_0 relative to the MOODS data in Fig. 10, we see that the ISOP2 synthetics have a slightly larger dense bias in the Gulf of Alaska, compared to the other test cases, including the HYCOM model cases. In other areas, ISOP2 is comparable to the other cases with a slightly smaller dense bias in the Greenland Sea. The bias for the HYCOM-05deg-lastdec appears to have the smallest overall bias, which is consistent because the last decade of data is closer in time to the validation dataset. Near the coast, in areas near a warm current, such as the Gulf Stream and the Alaskan Current, there tends to be a cold bias potentially due to anomalously warm water during this time period.

To see the difference over depth, we plot the T and S RMSE and bias error as a function of depth in Fig. 11. There are nearly 35 000 profiles down to 1000 m, decreasing in

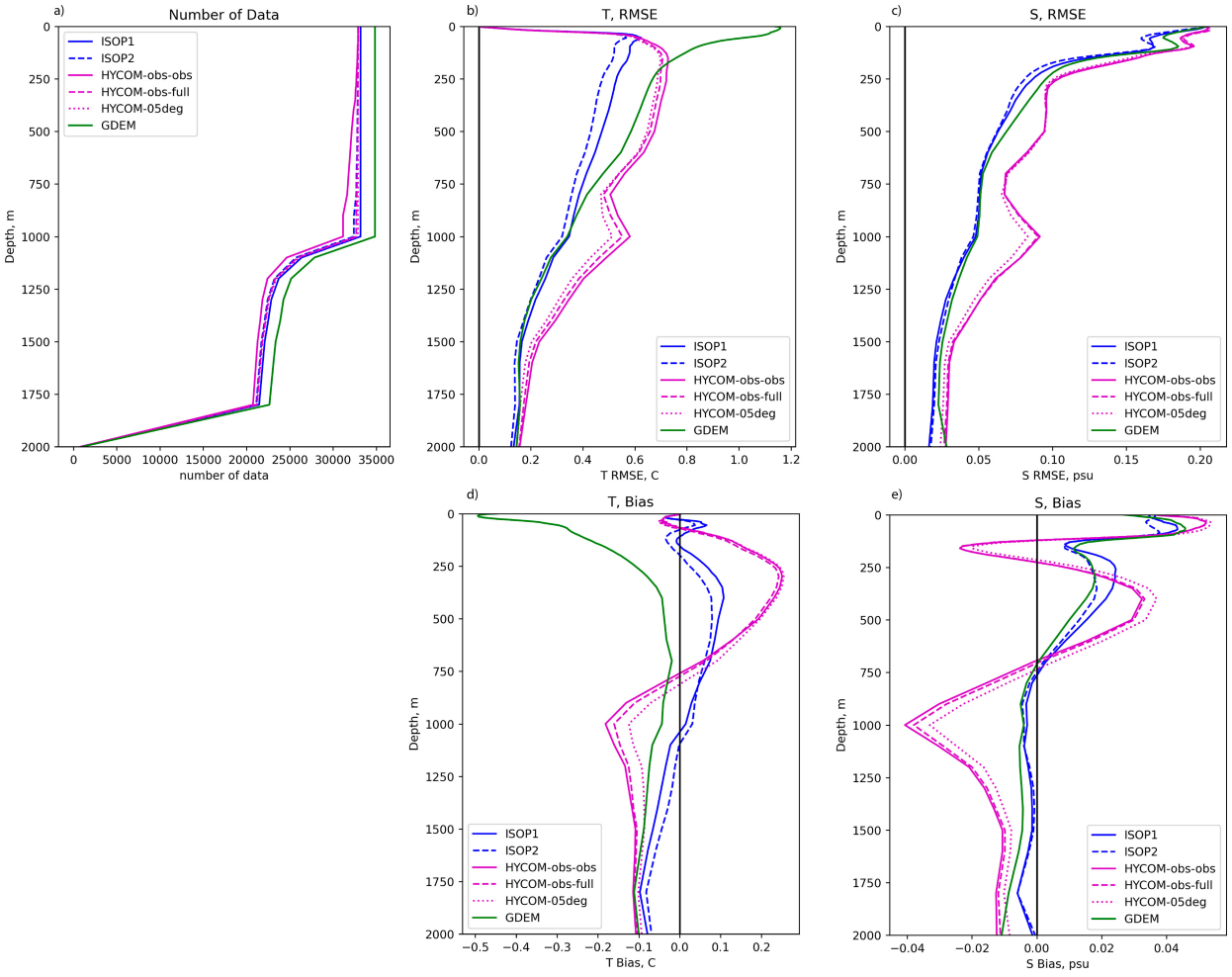

FIG. 11. The synthetic RMSE for (b) temperature and (c) salinity and bias for (d) temperature and (e) salinity vs depth relative to the MOODS in situ observations, for years 2019, 2020, and 2021, for 360° of longitude and northward of 60°N. (a) The number of observations vs depth, and the synthetic test cases are ISOP1, ISOP2, HYCOM-obs-obs, HYCOM-obs-full, and HYCOM-05deg, listed in the legend.

number at deep levels. We find over the Arctic Ocean and subarctic sea north of 60°N that the ISOP2 synthetics have the smallest T RMSE with ISOP1 being a close second. At deeper levels (below roughly 1000 m), the GDEM climatology has nearly the same T RMSE as the ISOP2 synthetics. The HYCOM cases have larger T RMSE over most of the water column. The HYCOM-obs-obs case has depth sampling like the ISOP1 case and has the largest RMSE. Notice that the GDEM case has a large negative T bias and T RMSE near the surface, whereas all others have small T errors near the surface. This is because the synthetics all have the profile SST as an input value, thus giving zero error at the surface. The GDEM case, however, does not have this advantage at the surface. In general, all vertical error covariance cases provide a viable database for creating synthetics.

SYNTHETIC VALIDATION IN REGIONS OF INTEREST

There are regions of interest evaluated in the companion paper (Douglass et al. 2026, unpublished manuscript) that use synthetics within the data assimilation system. Here, we evaluate synthetics relative to the MOODS data in three of those regions, one in the Labrador Sea (Fig. 12), the Bering Sea, and southwest (SW) of the Bering Sea (Figs. 13 and 14). We first evaluate the synthetic test cases, listed in Table 2, relative to the MOODS data in the five analysis boxes shown in Figs. 12d and 13d. In the Labrador Sea (Fig. 12), we find surprisingly that the GDEM climatology has the smallest RMSE and bias for depths 200 m and below; the green line in Figs. 12a, 12c, 12e, and 12f is closer to zero below 200 m, compared to the other lines in Fig. 12. The HYCOM-05deg case has a largest T RMSE near 1000–1500 m. At all other depths, the HYCOM-obs-obs case has the largest error. Even given the limited depth sampling of the HYCOM-obs-obs case, the RMSE and bias errors are still reasonable, compared to the other cases (solid magenta lines in Fig. 12). For salinity, the in situ cases ISOP1 and ISOP2 have a positive S bias for most of the water column below 250 m, whereas the HYCOM cases tend to have a negative S bias. For the case where the last

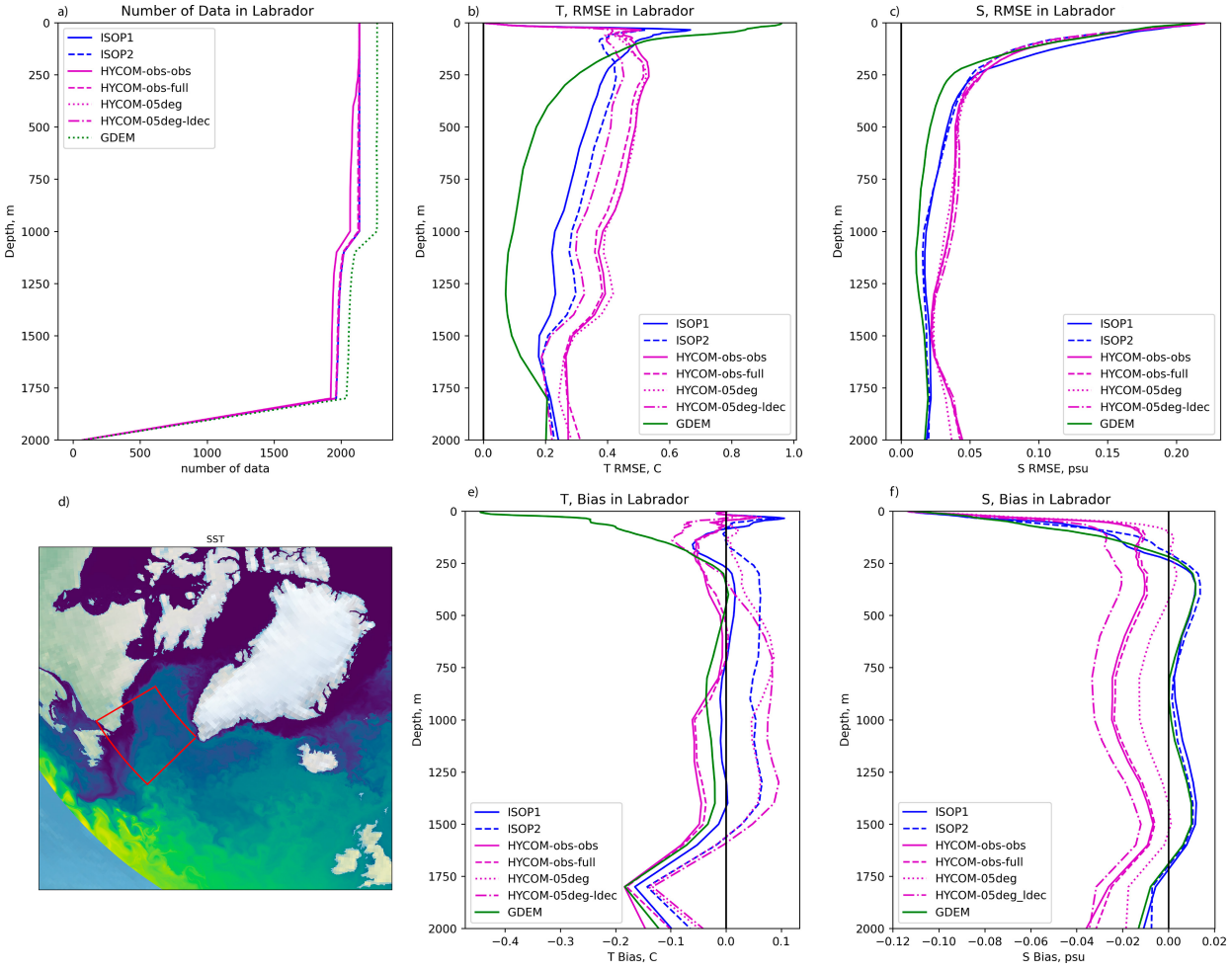

FIG. 12. The synthetic RMSE for (b) temperature and (c) salinity and bias for (e) temperature and (f) salinity vs depth relative to the MOODS in situ observations, for years 2019, 2020, and 2021, for (d) the Labrador Sea (red box). (a) The number of observations vs depth, and the synthetic test cases are ISOP1, ISOP2, HYCOM-obs-obs, HYCOM-obs-full, HYCOM-05deg, and HYCOM-05deg_ldec, listed in the legend.

decade of HYCOM data was used to create the vertical covariances, there is a larger warm bias (Fig. 12e) and fresh bias (Fig. 12f) in the Labrador Sea. In this region, the Labrador Sea box, there are numerous in situ observations for validation and to construct the vertical covariances; thus, the observation-derived synthetics outperform the model base synthetics. For the next two regions in the Bering Sea and just SW of the Bering Sea, we find that the model-based synthetics are as skillful as the observation-based cases.

In the Bering Sea, box 1 (Fig. 13), the synthetic errors are nearly the same for all vertical error covariance test cases. The largest differences occur in T RMSE above 250 m where the HYCOM cases have larger T RMSE and bias above 200 m, where the HYCOM case has a positive T bias and the ISOP1 and ISOP2 cases have a negative T bias (Fig. 13e). In the Bering Sea, there are far fewer observations for validation and constructing covariance; thus, the model-based synthetics are comparable. HYCOM-05deg-ldec, the case for the last decade of data, is comparable to other HYCOM cases but has the largest salinity bias below 200 m.

SW of the Bering Sea, box 2 (Fig. 14), the synthetic errors are even closer in value compared to box 1 for all vertical error covariance test cases. The largest outlier seems to be the GDEM cases that have larger T RMSE above 200 m and the GDEM T bias case for not having input SST near the surface. Again, HYCOM-05deg-ldec, the case for the last decade of data, is comparable to other HYCOM cases but has the largest salinity bias below 200 m.

b. *Synthetics in OSSE modeling system*

The main goal of this research is to create accurate, data assimilative ocean forecasts for the Arctic and subarctic seas, northward of 40°N. In a companion paper (Douglass et al. 2026, unpublished manuscript), an OSSE framework is utilized for examining the performance of an observational data assimilative ocean forecasting system. The OSSE experiments were designed to test the data assimilative system relative to a

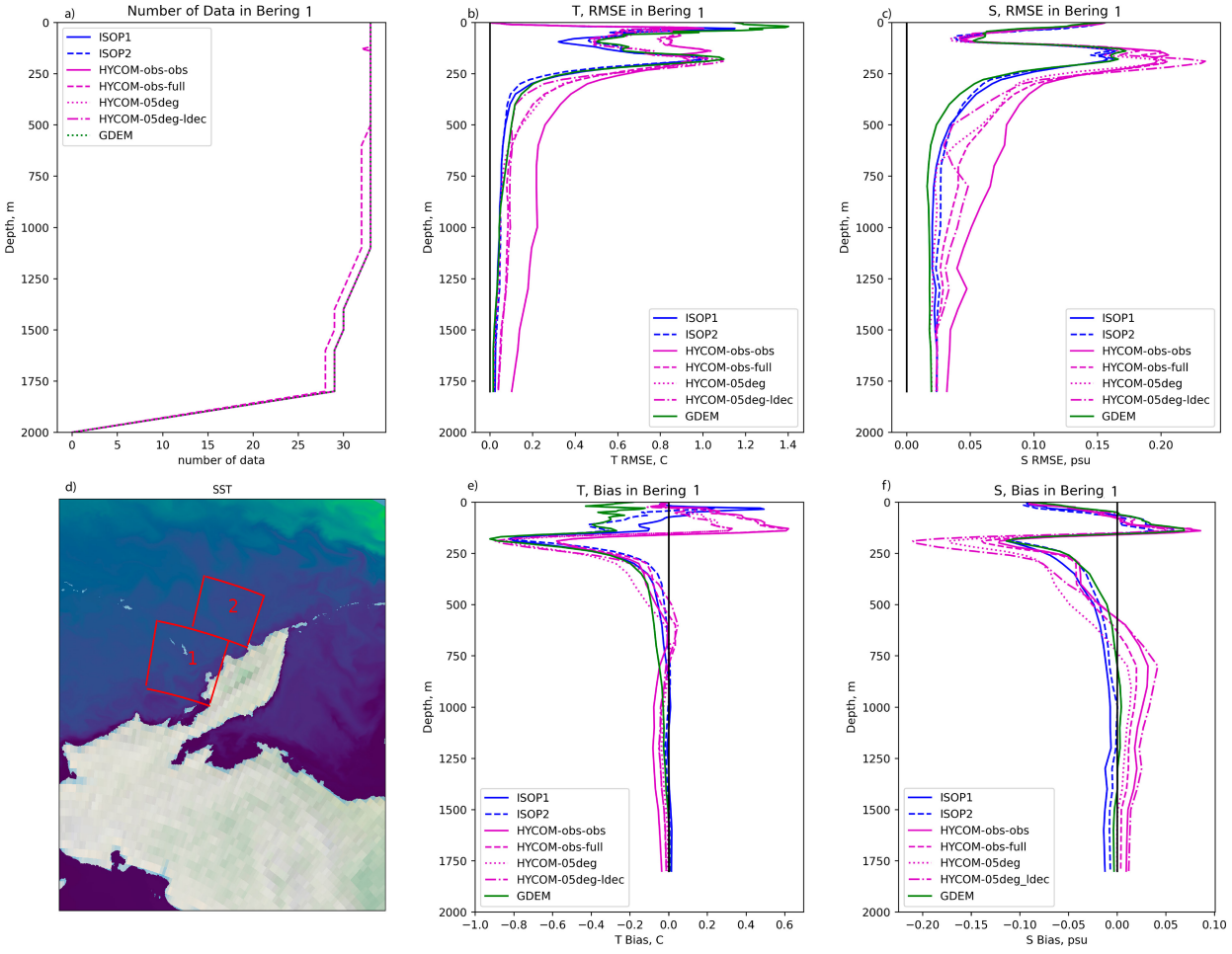

FIG. 13. The synthetic RMSE for (b) temperature and (c) salinity and bias for (e) temperature and (f) salinity vs depth relative to the MOODS in situ observations, for years 2019, 2020, and 2021, for (d) the Bering Sea in the box labeled "1." (a) The number of observations vs depth, and the synthetic test cases are ISOP1, ISOP2, HYCOM-obs-obs, HYCOM-obs-full, HYCOM-05deg, and HYCOM-05deg_ldec, listed in the legend.

simulated ocean called the nature run. In the OSSEs, the nature run is a global ocean/sea ice model that uses the Parallel Ocean Program, version 2 (POP2), model with the Los Alamos Sea Ice Model, version 5 (CICEv5) (Hunke et al. 2015), coupled together in the U.S. Department of Energy (DOE)'s Energy Exascale Earth System Model "HiLAT" framework (E3SMv0-HiLAT) (Hecht et al. 2019). The model's horizontal grid is configured to have nominal resolution close to 8 km at the equator reducing to 2 km at the poles. The initial conditions for POP were taken from the Navy's 1/25° Global Ocean Forecasting System, version 3.5 (GOFS3.5) (Metzger et al. 2020), system, and the atmospheric forcing used is the Japanese 55-year Reanalysis-driving ocean (JRA-55-do) (Tsujino et al. 2018). Further details about the nature Run can be found in Fine et al. (2023).

Using the OSSE framework, experimental test cases using HYCOM were created. This implementation of HYCOM was also coupled with CICEv5. The OSSE member had a resolution of 1/12° at the equator and is roughly 4 km at the poles. The region used here is known as the Arctic Cap, including all latitudes north of 40°N. Each OSSE was run for 1 year, starting on 1 January 2017. The initial and boundary conditions are from the Navy's operational system for the ocean state (Chassignet et al. 2009; Metzger et al. 2014), and the atmospheric forcing is from the Navy Global Environmental Model (NAVGEM) (Hogan et al. 2014). The OSSE modeling configuration is different from the nonassimilative simulations used to create the vertical covariances (Chassignet et al. 2020). This could introduce some bias errors into the synthetics from drift of the free-running HYCOM simulation used to create the vertical covariances.

HYCOM-BASED SYNTHETICS IN OSSE

MODELING SYSTEM

To evaluate the model-based synthetic performance within a cycling data assimilation system, we performed two OSSEs using the framework described in the introduction of section 3b. The first OSSE case (OSSE-ISOP1) uses ISOP1 synthetics and represents the present operational capability as described in

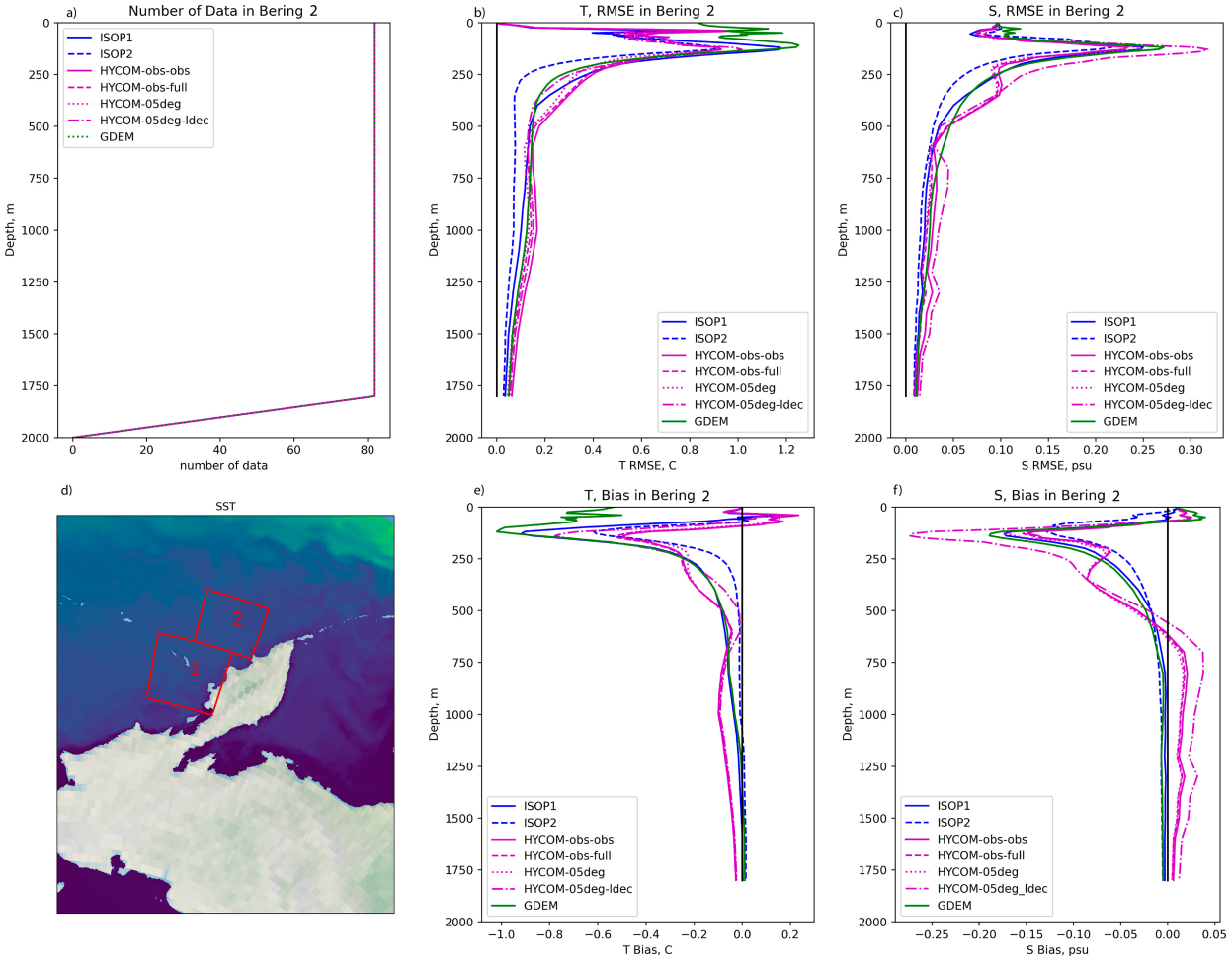

FIG. 14. The synthetic RMSE for (b) temperature and (c) salinity and bias for (e) temperature and (f) salinity vs depth relative to the MOODS in situ observations, for years 2019, 2020, and 2021, (d) SW of the Bering Sea in the box labeled "2." (a) The number of observations vs depth, and the synthetic test cases are ISOP1, ISOP2, HYCOM-obs-obs, HYCOM-obs-full, HYCOM-05deg, and HYCOM-05deg-ldec, listed in the legend.

Douglass et al. (2026, unpublished manuscript). The second OSSE case (OSSE-HYCOM-05deg) in this manuscript uses the synthetics derived from HYCOM-05deg vertical error covariances (see Table 1). The data sampling selection includes all available SSH data locations and does not exclude synthetic profiles if the vertical ocean stratification is small, where the difference in temperature between 1000 and the surface is less than 3°C (see Fig. 2). This new OSSE member was run for 1 year, starting on 1 January 2017, and the results included here are for 1 day, 31 December of 2017.

To evaluate the performance of this OSSE experimental test case, we evaluate it relative to the POP2 nature run in the three boxes of interest used above, in the Labrador Sea, the Bering Sea, and SW of the Bering Sea (Figs. 15–17). We compute the spatial average over the box domains for the nature run, climatology, and the OSSE-ISOP1 and OSSE-HYCOM-05deg experiments. In OSSE-ISOP1, the profiles are close to GDEM and the OSSE is not able to emulate the nature run since SSH data assimilation of synthetics will bring the solution closer toward the synthetic climatology, ISOP1 in this case. This is seen in all three figures (Figs. 15–17), where the red lines and the black lines are closer together, compared to the others. In the OSSE-HYCOM-05deg case, the profiles are closer to the nature run (blue and green lines tend to be closer together in Figs. 15–17) because the synthetics represent the time evolution of the global nonassimilative HYCOM model as it evolves away from the GDEM initial conditions (Chassignet et al. 2020) as it is the case for the POP nature run. In the Labrador Sea, OSSE-HYCOM-05deg is closer to OSSE-ISOP1 and GDEM than to the nature run (Fig. 15). In boxes 1 and 2 in and near the Bering Sea, OSSE-HYCOM-05deg is closer to the nature run as both HYCOM and the nature run are not able to represent the temperature inversion present in this region (Figs. 16 and 17). In this case, the GDEM climatology is far from the POP2 nature run SW of the Bering Sea.

c. *Analysis of synthetic errors on T versus S diagrams*

To evaluate the effectiveness of limiting the use of synthetics at high latitude (northward of 50°N) based on stratification

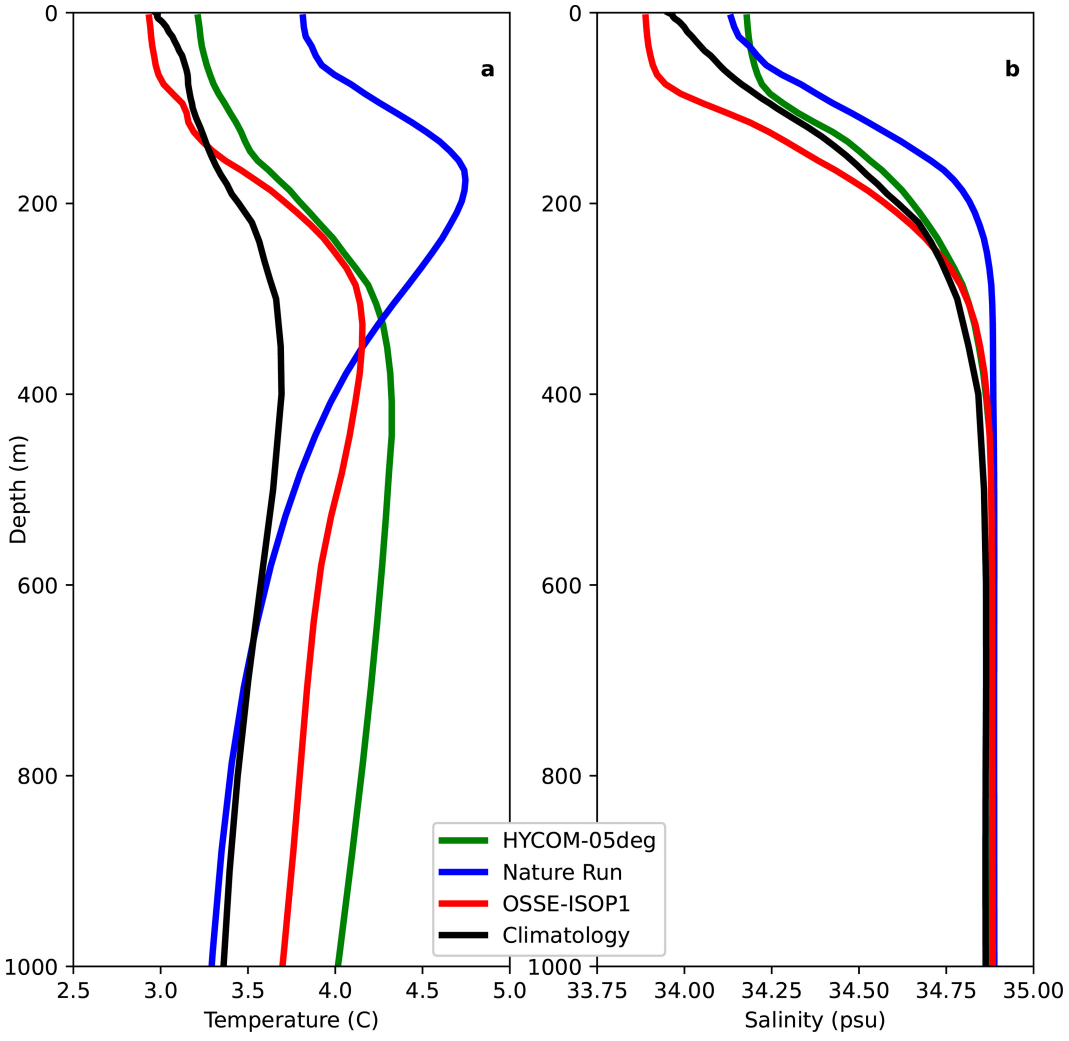

FIG. 15. The spatial average, in the Labrador Sea in box (see Fig. 12d), vs depth of (a) temperature and (b) salinity for OSSE member OSSE-HYCOM-05deg (green line) utilizing the HYCOM-05deg vertical error covariance and OSSE-ISOP1 (red line) to create synthetics. The blue line is the Nature run and the black line is GDEM climatology. The results here are for 1 day, 31 Dec 2017.

(see the introduction and Fig. 2), we compute histograms, weighted by density RMS error on T versus S diagrams. In Fig. 18, there are three types of two-dimensional (2D) histograms. The result provides an estimate of the rate of error in each bin. Because the stratification test is computed from the synthetics as the temperature difference between the surface and 1000 m, we create bins that cover the difference in T and S from the surface to 1000 m (see Fig. 18). The histogram in Fig. 18a shows the number of profiles with the corresponding T and S difference between 0- and 1000-m depth. Figure 18b weights each one by the RMS error with depth of the profile σ_0. In Figs. 18c–e, we have the ratio of panels a and b for the ISOP1, ISOP2, and HYCOM last decade test cases.

We can see that there are areas where the difference in temperature from the surface to 1000-m depth has relatively good synthetics for low T stratification. The cutoff in the present system is 3°C. In this case, the region in these plots on the y axis from −3° to 3°C would be eliminated (green lines in Fig. 18c). Clearly, this threshold is too strict and often wrong, as low T stratification is not a good indicator of synthetics quality. Instead, salinity stratification may be a better indicator, which we explore next.

Because the ocean at 1000 m is relatively unchanging compared to the upper ocean, we can ignore the 1000-m synthetic values for evaluating the veracity of the synthetics. If we consider the two-dimensional histograms using just the surface values with 50 evenly spaced bins of temperature from −1.8° to 20.0°C and 50 evenly spaced bins of salinity from 30.25 to 35.9 psu, the result is in Fig. 19. Thus, the primary variable for evaluating the skill of synthetics is the surface values, which are controlled primarily by the input SST and climatological S, since surface salinity is not an input. The synthetic values of T and S at 1000 m do not change enough for them to be a major factor. In Fig. 20, we show the same calculation in each of

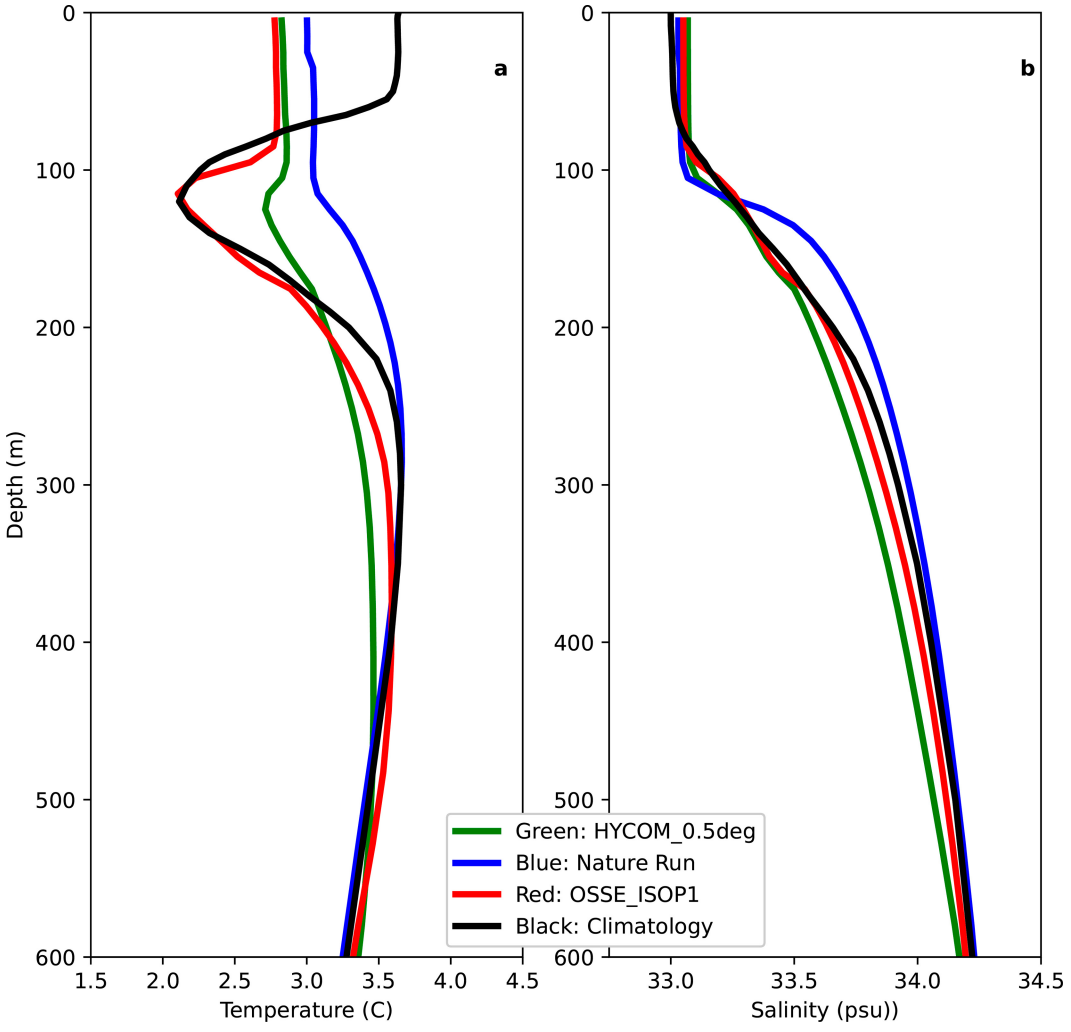

FIG. 16. The spatial average, in the Bering Sea in box 1 (see Fig. 13d), vs depth of (a) temperature and (b) salinity for OSSE member OSSE-HYCOM-05deg (green line) utilizing the HYCOM-05deg vertical error covariance and OSSE-ISOP1 (red line) to create synthetics. The blue line is the nature run, and the black line is climatology.

the regions of interest for the Labrador (see Fig. 12) and Bering (see Fig. 13) Seas. For the Bering Sea, there are not many profiles, but the synthetics have relatively good performance relative to other regions.

d. Determine T/S areas of synthetics quality

To determine when synthetics are skillful, the observation error for the synthetics can be determined by only the surface values of the synthetics. The rule seems to be dependent on the region of the ocean. The T versus S areas where synthetics are more skillful is different in the North Atlantic compared to the North Pacific. In fact, it seems that the skill of the synthetics depends mostly on salinity. If we simply select a salinity value of 35 psu for the Atlantic Ocean and 32.4 psu for the Pacific Ocean, we see that many of the synthetics are skillful near these values (see Fig. 19). This is a curious finding given the fact that surface salinity is not an input parameter for making synthetics (see section 2 and the appendix). Future systems should have the error level associated with the synthetic be dependent on surface salinity.

Another potential criterion to determine synthetic error levels is the deviation from the climatological T value at the location of the synthetic. Since there is no input S for creating synthetics, the surface S for the salinity is very close to the climatological value. The T value, however, varies according to the input SST values. Evaluating this relative to the climatological value reveals an interesting relationship (Fig. 21). The synthetics have a higher rate of error for input SST values that are far from the climatological value. This suggests that synthetics are more accurate when the SST is close to the climatology value. Thus, the vertical covariances are most representative of the observed ocean.

4. Conclusions

This paper describes research aimed at creating accurate, data assimilative ocean forecasts for the Arctic and subarctic

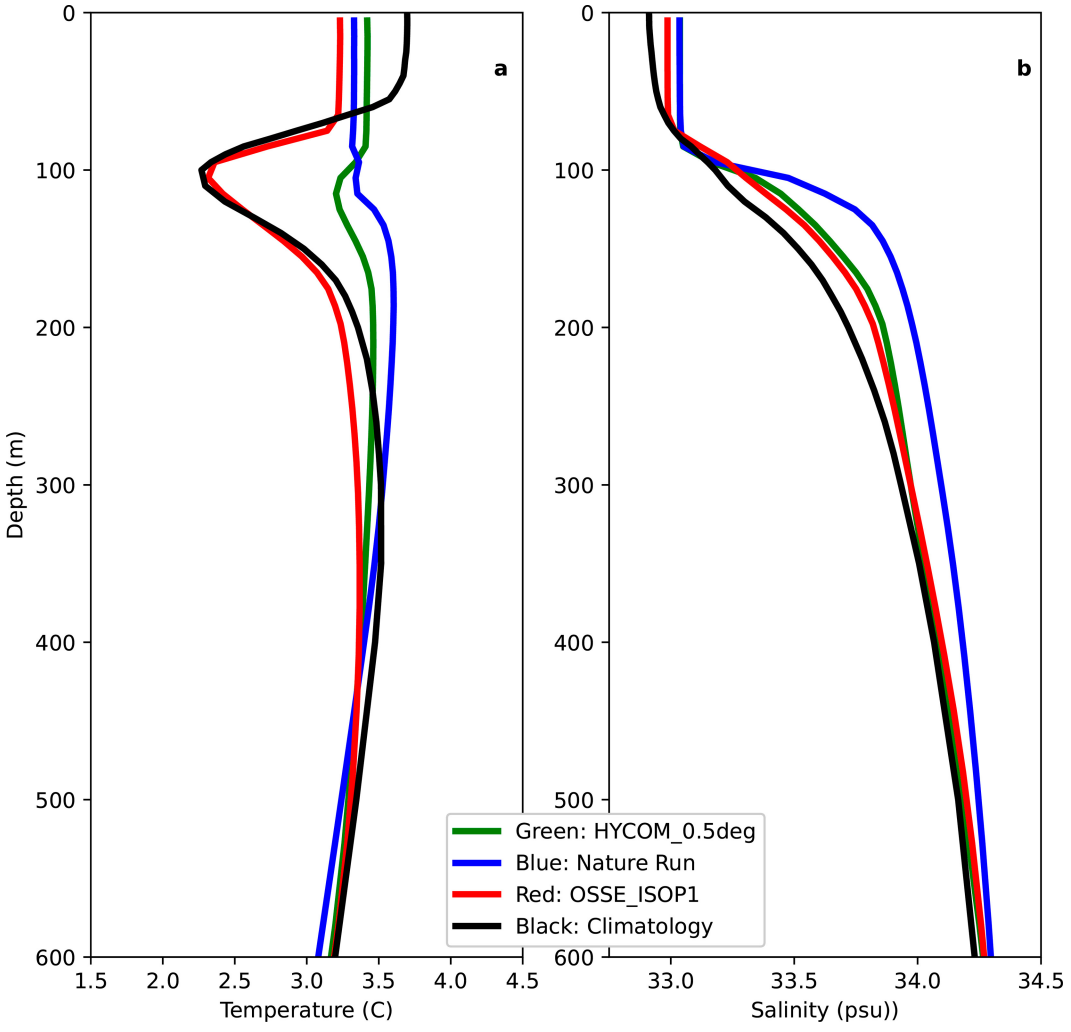

FIG. 17. The spatial average, SW of the Bering Sea in box 2 (see Fig. 14d), vs depth of (a) temperature and (b) salinity for OSSE member OSSE-HYCOM-05deg (green line) utilizing the HYCOM-05deg vertical error covariance and OSSE-ISOP1 (red line) to create synthetics. The blue line is the nature run, and the black line is climatology.

seas. We focus on the usage of SSHA data in the creation of synthetic ocean profiles. Synthetic profiles represent the subsurface ocean structure associated with the observed SSHA, SST, and input MLD. These profiles are then assimilated into the ocean model. Historically, the use of synthetics has been restricted at high latitude due to degraded accuracy. To address this issue, the present analysis utilizes model data as a substitute for in situ–observed profiles in creating vertical error covariances of temperature and salinity for making synthetics. The present analysis explores the effectiveness of this approach and suggests an improved synthetic error estimation.

Using the model data, we focus on six different versions of the covariances, two that come from in situ observations and four derived from HYCOM ocean model simulations. The advantage of using model data is the uniform coverage of the global ocean in space and time, including at high latitude where in situ observations are sparse. The results of this analysis suggest that model data are a suitable replacement for where and when in situ observations are not present. All cases present a viable option for application in an operational ocean data assimilation system. In general, the observation-based vertical covariances result in synthetics with smaller RMSE and bias, except near the surface, compared to the model-based covariances. In regions of the ocean where there are few in situ observations, such as the Bering Sea, the model-based covariances had similar RMSE and bias, when creating synthetics, compared to the observation-based covariances. For the case where the last decade of HYCOM data was used to create the vertical covariances, the overall result was to reduce the bias error. Looking in the small subregions, however, there is a larger warm bias and fresh bias in the Labrador Sea and in the Bering Sea, and the last decade of data increased the salinity bias below 750 m.

As described in section 2c, the model-derived covariance test cases have a slight disadvantage compared to the in situ–derived covariance cases. The disadvantage is due to the

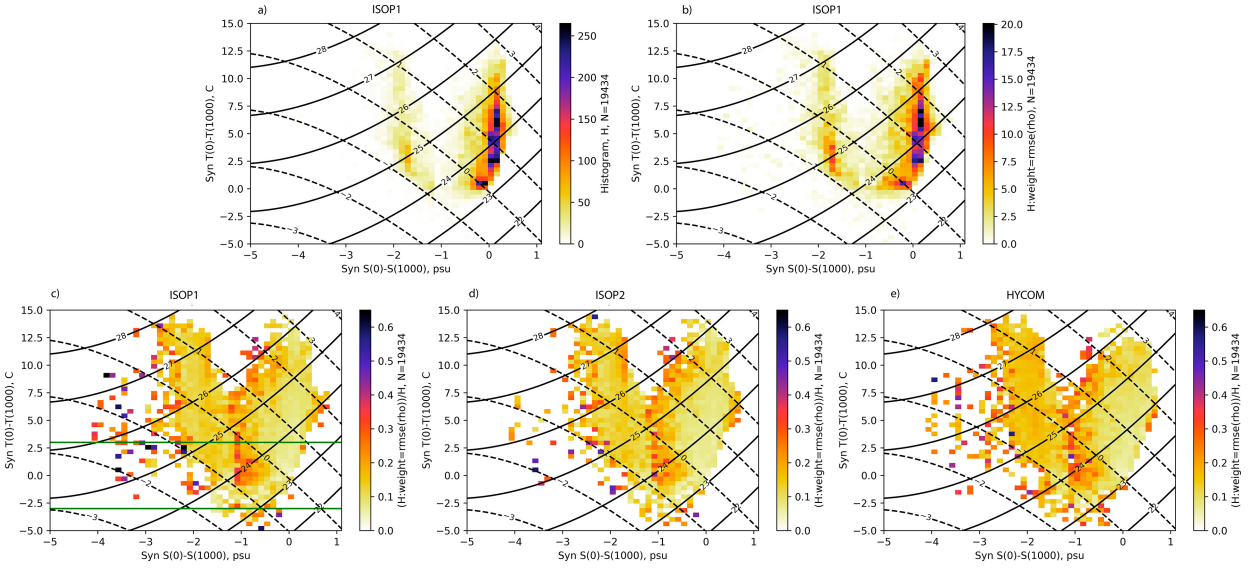

FIG. 18. Histograms of the (a) number of profiles, (b) number of profiles weighted by the density RMSE over depth of the synthetics, and the ratio of (a) and (b) for the (c) ISOP1, (d) ISOP2, and (e) HYCOM last decade test cases. Panels represent the rate of error for the synthetics compared to in situ observations northward of 50°N. The histogram is sorted in bins of the difference from the surface to 1000 m for T and S. For T, there are 50 evenly spaced bins from −5° to 15°C, and for S, there are 50 evenly spaced bins from −5 to 1.1 psu. The solid contour lines are surface reference potential density σ_θ, and the dashed contour lines are potential spiciness referenced to the surface (McDougall and Krzysik 2015).

derivation of the climatological-mean steric height values. In the in situ observation test case, ISOP1, the in situ–derived monthly climatological- and annual-mean steric height data are identical to those used to derived vertical error covariances. In all other cases, the same in situ–derived annual-mean steric height data are used. The monthly climatological-mean steric height data, however, come from the model data itself. This inconsistency is minor since the monthly climatological-mean anomaly is separate from the annual-mean anomaly. The system equates the anomalies, not the total steric height. In addition, the HYCOM model itself is initialized from the same data as that for the annual-mean steric height.

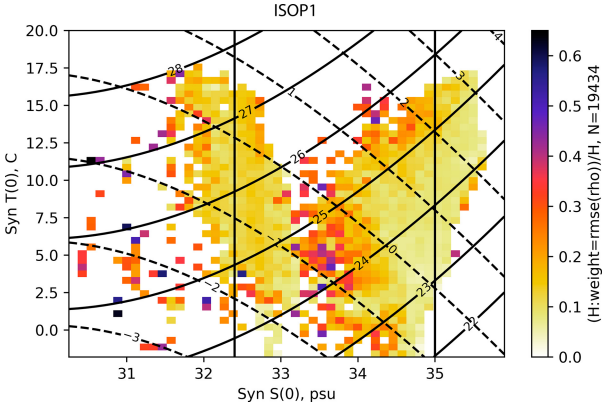

FIG. 19. Histograms of the ratio of the number of profiles to the number of profiles weighted by the density RMSE over the depth of the synthetics for the ISOP1 test case. The bins are sorted by the surface T and S values of the synthetic profiles with 50 evenly spaced bins of temperature ranging from −1.8° to 20.0°C and 50 evenly spaced bins of salinity ranging from 30.25 to 35.9 psu. The contour lines are as in Fig. 18. The straight vertical black lines are at 32.4 and 35.0 psu.

A motivating factor for using model data as a source of ocean covariances is the time and space sampling, which is superior to that of available in situ observations. Because of the limited observations, particularly at high latitude, present Navy ocean data assimilation systems restrict the use of synthetic profiles at high latitudes (Douglass et al. 2026, unpublished manuscript). A goal of this research is to extend synthetic usage to higher latitude using model-derived vertical error covariances. The present analysis shows that model-derived synthetics perform accurately in the Bering and Labrador Seas. In the central Arctic, however, there is a negative cross correlation between T and S in the ISOP2 dataset, whereas the HYCOM-obs-obs and the HYCOM_05deg cases have a positive cross correlation. Since HYCOM has opposite correlations, the solution may not work correctly in the central Arctic. For the evaluation relative to independent observations, there were no independent data (after the period for creating covariances) that satisfied the criteria requiring data to extend down to 1000 m in the central Arctic Ocean, and thus, we were unable to evaluate the system there. In addition, Baffin Bay is another region where the HYCOM data have an opposite T/S cross correlation to that of the ISOP1 dataset.

Since the inputs for making synthetics include SST, SSH and MLD, salinity is only controlled by the error covariances and not through inputs. For this reason, the salinity errors were relatively equal among the test cases. In the Labrador

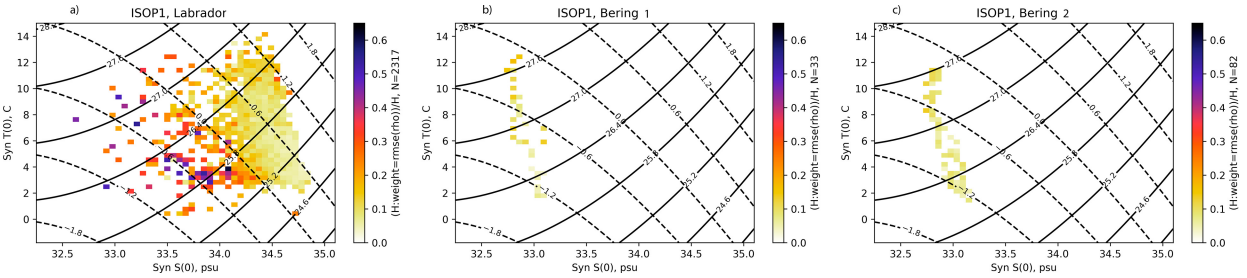

FIG. 20. Histograms of the ratio of the number of profiles to the number of profiles weighted by the density RMSE over the depth of the synthetics for the ISOP1 test case. The bins are as in Fig. 19. (a) The Labrador Sea box, (b) the Bering Sea box 1, and (c) the SW of Bering Sea box 2. The contour lines are as in Fig. 18.

Sea, the salinity bias is opposite for the in situ–derived versus the HYCOM-model-derived test cases.

In corroboration with the findings in the companion paper (Douglass et al. 2026, unpublished manuscript), the accuracy of the climatological-mean structure used in the construction of the synthetics is crucial to the results, as shown in the OSSE experiment. Thus, inaccurate climatological-mean state in the synthetic database will inject those inaccuracies in the model prediction.

We find that the accuracy of the synthetics is strongly related to the surface salinity of the synthetics, particularly when the ocean deviates from climatology. Since there is no salinity input for creating synthetics, the surface salinity of the synthetics is nearly identical to climatology. Thus, maps of good synthetics skill can be determined from maps of climatology surface salinity. This finding suggests that observations of salinity, if incorporated into the system, could substantially improve the accuracy of synthetics.

For future applications, the model-derived solution could be used everywhere except potentially the central Arctic and Baffin Bay. Due to few available in situ observations for validation, however, we are unable to validate the system in those locations. This method would be particularly useful in regions with few data such as the central Arctic Ocean, Sea of Okhotsk, or Baffin Bay, provided the model solution is correct. The bias reduction found for the case HYCOM-last-decade suggests that creating a new climatology from more recent data would improve the quality of the synthetics. Improving the annual mean by removing the mesoscale variability in the analysis process (Wijffels et al. 2024) would likely help the RMSE for the synthetics.

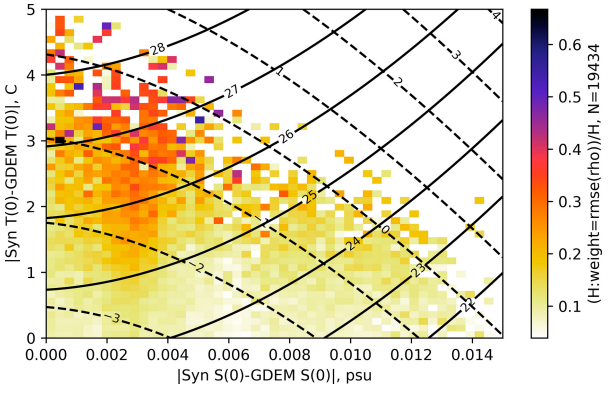

FIG. 21. Histograms of the rate of error computed as ratio of the number of profiles to the number of profiles weighted by the density RMSE over the depth of the synthetics for the ISOP1 test case. The histogram is sorted in bins of the difference of the synthetic from GDEM climatology. For T, there are 50 evenly spaced bins ranging from 0° to 5°C, and for S, there are 50 evenly spaced bins ranging from 0 to 0.014 psu. The contour lines are as in Fig. 18.

Acknowledgments. This work was performed with funding from the National Ocean Partnership Program, under a project entitled "Arctic Observing System Simulation Experiments (OSSEs) within the ONR/Navy Global Ocean Forecasting System (GOFS) and Earth System Prediction Capability (ESPC) frameworks" led by Florida State University, Project N00014-19-12674. In addition to the NOPP funding, J. McClean (UCSD/SIO) was supported by Office of Naval Research (ONR) Award N00014-24-12541. The Naval Research Laboratory also received additional funding from ONR Award 73-1D57-13-5 and program manager Scott L. Harper. The nature run used in this study was produced at the U.S. Army Engineer Research and Development Center (ERDC) Department of Defense (DoD) Supercomputing Resource Center (DSRC) using computing resources from the DoD High-Performance Computing Modernization Program (HPCMP). This paper is Contribution NRL/7320/JA-2025/2 and has been approved for public release.

Data availability statement. The authors do not have permission to release the data and software to the public.

APPENDIX

The 1D Synthetic Model Formulation

The system for constructing synthetic profiles from surface observations of sea surface temperature, $\tilde{T}_1$, and height anomaly, $\delta\tilde{h}$, has a dynamic layer constrained by empirically derived vertical covariances (Helber et al. 2013). The cost function, to create one synthetic profile at a location, is given by

$$J = [\delta\mathbf{x}^{(\mathrm{clim})}]^{\mathrm{T}}\mathbf{B}^{-1}[\delta\mathbf{x}^{(\mathrm{clim})}] + [\delta\mathbf{d}^{(\mathrm{clim})}]^{\mathrm{T}}[\mathbf{B}^{(d)}]^{-1}[\delta\mathbf{d}^{(\mathrm{clim})}] + [\delta\mathbf{x}^{(\mathrm{eof})}]^{\mathrm{T}}\mathbf{V}^{-1}[\delta\mathbf{x}^{(\mathrm{eof})}] + [\delta\mathbf{d}^{(\mathrm{eof})}]^{\mathrm{T}}[\mathbf{V}^{(d)}]^{-1}[\delta\mathbf{d}^{(\mathrm{eof})}] + [\delta\tilde{T}_1^{(\mathrm{obs})}][R^{(\mathrm{SST})}]^{-1}[\delta\tilde{T}_1^{(\mathrm{obs})}] + [\mathbf{L}\delta\mathbf{x}^{(\mathrm{clim})} - \delta\tilde{h}^{(\mathrm{clim})}] \times (R^{(\mathrm{SSHA})})^{-1}[\mathbf{L}\delta\mathbf{x}^{(\mathrm{clim})} - \delta\tilde{h}^{(\mathrm{clim})}]. \quad \text{(A1)}$$

The first term involves the anomaly of the synthetic solution from the climatological profile, for the month, at the profile's location given by

$$\delta\mathbf{x}^{(\mathrm{clim})} = \mathbf{x} - \mathbf{x}^{(\mathrm{clim})}, \quad \text{(A2)}$$

where

$$\mathbf{x} = \begin{bmatrix} T_{k_{\mathrm{mld}}} & T_{k_{\mathrm{mld}}+1} & \cdots & T_{\mathrm{nz}} & S_{k_{\mathrm{mld}}} & S_{k_{\mathrm{mld}}+1} & \cdots & S_{\mathrm{nz}} \end{bmatrix}, \quad \text{(A3)}$$

and T and S are the synthetic temperatures and salinity, respectively, at depths k_{mld}, $k_{\mathrm{mld}} + 1$, and $k_{\mathrm{mld}} + 2$, etc., down to the last depth grid nz, where k_{mld} is the index of the analysis grid below the input mixed layer depth (MLD). Now, $\mathbf{x}^{(\mathrm{clim})}$ has the same form but with climatological values:

$$\mathbf{x}^{(\mathrm{clim})} = \begin{bmatrix} T^{(\mathrm{clim})}_{k_{\mathrm{mld}}} & T^{(\mathrm{clim})}_{k_{\mathrm{mld}}+1} & \cdots & T^{(\mathrm{clim})}_{\mathrm{nz}} & S^{(\mathrm{clim})}_{k_{\mathrm{mld}}} & S^{(\mathrm{clim})}_{k_{\mathrm{mld}}+1} \cdots S^{(\mathrm{clim})}_{\mathrm{nz}} \end{bmatrix}. \quad \text{(A4)}$$

The second term involves the anomaly of the synthetic solution vertical gradient from the climatological profile vertical gradient, for the month, at the profile's location given by

$$\delta\mathbf{d}^{(\mathrm{clim})} = \mathbf{d} - \mathbf{d}^{(\mathrm{clim})}, \quad \text{(A5)}$$

where the gradients are computed as the difference between two depth levels:

$$\mathbf{d} = \begin{bmatrix} \Delta T_{k_{\mathrm{mld}}} & \Delta T_{k_{\mathrm{mld}}+1} & \cdots & \Delta T_{\mathrm{nz}-1} & \cdots \\ \Delta S_{k_{\mathrm{mld}}} & \Delta S_{k_{\mathrm{mld}}+1} & \cdots & \Delta S_{\mathrm{nz}-1} & \end{bmatrix}, \quad \text{(A6)}$$

where $\Delta T_k = T_{k+1} - T_k$ and $\Delta S_k = S_{k+1} - S_k$. The terms including $\mathbf{d}^{(\mathrm{clim})}$ have the same form but with climatological values:

$$\mathbf{d}^{(\mathrm{clim})} = \begin{bmatrix} \Delta T^{(\mathrm{clim})}_{k_{\mathrm{mld}}} & \Delta T^{(\mathrm{clim})}_{k_{\mathrm{mld}}+1} & \cdots & \Delta T^{(\mathrm{clim})}_{\mathrm{nz}-1} & \cdots \\ \Delta S^{(\mathrm{clim})}_{1k_{\mathrm{mld}}} & \Delta S^{(\mathrm{clim})}_{k_{\mathrm{mld}}+1} & \cdots & \Delta S^{(\mathrm{clim})}_{\mathrm{nz}-1} & \end{bmatrix}, \quad \text{(A7)}$$

where $\Delta T^{(\mathrm{clim})}_k = T^{(\mathrm{clim})}_{k+1} - T^{(\mathrm{clim})}_k$ and $\Delta S^{(\mathrm{clim})}_k = S^{(\mathrm{clim})}_{k+1} - S^{(\mathrm{clim})}_k$. The background vertical error covariance, for this location and month, is

$$\mathbf{B} = \mathbf{UCU}, \quad \text{(A8)}$$

where the climatological standard deviation is $\mathbf{U}$ and climatologically derived correlation is $\mathbf{C}$. We compute the analogous background error covariance for the vertical gradient of the synthetic values given by

$$\mathbf{B}^{(d)} = \mathbf{U}^{(d)}\mathbf{C}^{(d)}\mathbf{U}^{(d)}, \quad \text{(A9)}$$

where the climatological standard deviation is $\mathbf{U}^{(d)}$ and climatologically derived correlation is $\mathbf{C}^{(d)}$, computed from vertical gradients in T and S as in Eq. (A7). The Navy's Master Oceanographic Observation Dataset (MOODS) (Bauer 1985; Teague et al. 1987) is the in situ profile database used to create $\mathbf{B}$ and $\mathbf{B}^{(d)}$. We separate the correlations into four components such that

$$\mathbf{C} = \begin{bmatrix} \mathbf{C}^{(T-T)} & \mathbf{C}^{(T-S)} \\ \mathbf{C}^{(T-S)} & \mathbf{C}^{(S-S)} \end{bmatrix} \text{and } \mathbf{C}^{(d)} = \begin{bmatrix} \mathbf{C}^{(d)(T-T)} & \mathbf{C}^{(d)(T-S)} \\ \mathbf{C}^{(d)(S-T)} & \mathbf{C}^{(d)(S-S)} \end{bmatrix}, \quad \text{(A10)}$$

where $\mathbf{C}^{(T-T)}$, $\mathbf{C}^{(S-S)}$, $\mathbf{C}^{(d)(T-T)}$, and $\mathbf{C}^{(d)(S-S)}$ are the autocorrelations for T and S and $\mathbf{C}^{(T-S)}$, $\mathbf{C}^{(S-T)}$, $\mathbf{C}^{(d)(T-S)}$, and $\mathbf{C}^{(d)(S-T)}$ are the cross correlations for T and S and the transposes for each. Figure 3 shows the vertical correlation $\mathbf{C}$, and Fig. A1 shows the vertical gradient correlations $\mathbf{C}^{(d)}$. The data in Figs. 3 and A1 are valid at a location in the Lofoten Basin within the Norwegian Sea.

The terms on the second line of Eq. (A1) constrain the synthetic profile to the reduced EOF mode representation of the climatological vertical profile. Those terms are normalized by the climatological variances by $\mathbf{V}$ and $\mathbf{V}^{(d)}$. For computational efficiency and to reduce data storage, the full correlations, $\mathbf{C}$, for the global ocean at 1/2° resolution represented by a six-mode Jordan decomposition are given by (e.g., Strang 2006)

$$\mathbf{B} = \mathbf{U}\boldsymbol{\Gamma}\boldsymbol{\Lambda}\boldsymbol{\Gamma}^{\mathrm{T}}\mathbf{U}, \quad \text{(A11)}$$

where $\boldsymbol{\Lambda}$ is a diagonal matrix with elements, λ_i, equal to the singular values of $\mathbf{C}$. The columns of the orthogonal matrix, $\boldsymbol{\Gamma}$, are the combined T and S eigenvectors, γ_i, of $\mathbf{C}$. From the EOF decomposition, we construct amplitudes given by

$$\mathbf{a} = \boldsymbol{\Gamma}^{\mathrm{T}}\mathbf{U}^{-1}[\mathbf{x} - \mathbf{x}^{(\mathrm{clim})}], \quad \text{(A12)}$$

and for the vertical gradient,

$$\mathbf{a}^{(d)} = \boldsymbol{\Gamma}^{(d)\mathrm{T}}\mathbf{U}^{(d)^{-1}}[\mathbf{d} - \mathbf{d}^{(\mathrm{clim})}]. \quad \text{(A13)}$$

Using six modes of eigenvectors and eigenvalues, the first term on the second line of Eq. (A1) has

$$\delta\mathbf{x}^{(\mathrm{eof})} = \mathbf{U}\boldsymbol{\Gamma}^{(6)}\mathbf{a}^{(6)}. \quad \text{(A14)}$$

Similarly, for the vertical gradient constraint, we have

$$\delta\mathbf{d}^{(\mathrm{eof})} = \mathbf{U}^{(d)}\boldsymbol{\Gamma}^{(d:6)}\mathbf{a}^{(d:6)}. \quad \text{(A15)}$$

The first term on the third line of Eq. (A1) is the SST term, which has

$$\delta\tilde{T}_1{}^{(\mathrm{obs})} = \tilde{T}_1 - \tilde{T}^{(\mathrm{SST})}, \quad \text{(A16)}$$

where T_1 is the first-level synthetic temperature in Eq. (A1) and $\tilde{T}^{(\mathrm{SST})}$ is the input observed sea surface temperature (SST) value. The $R^{(\mathrm{SST})}$ in Eq. (A1) is the error estimate for SST, which include representation errors, not just instrument error.

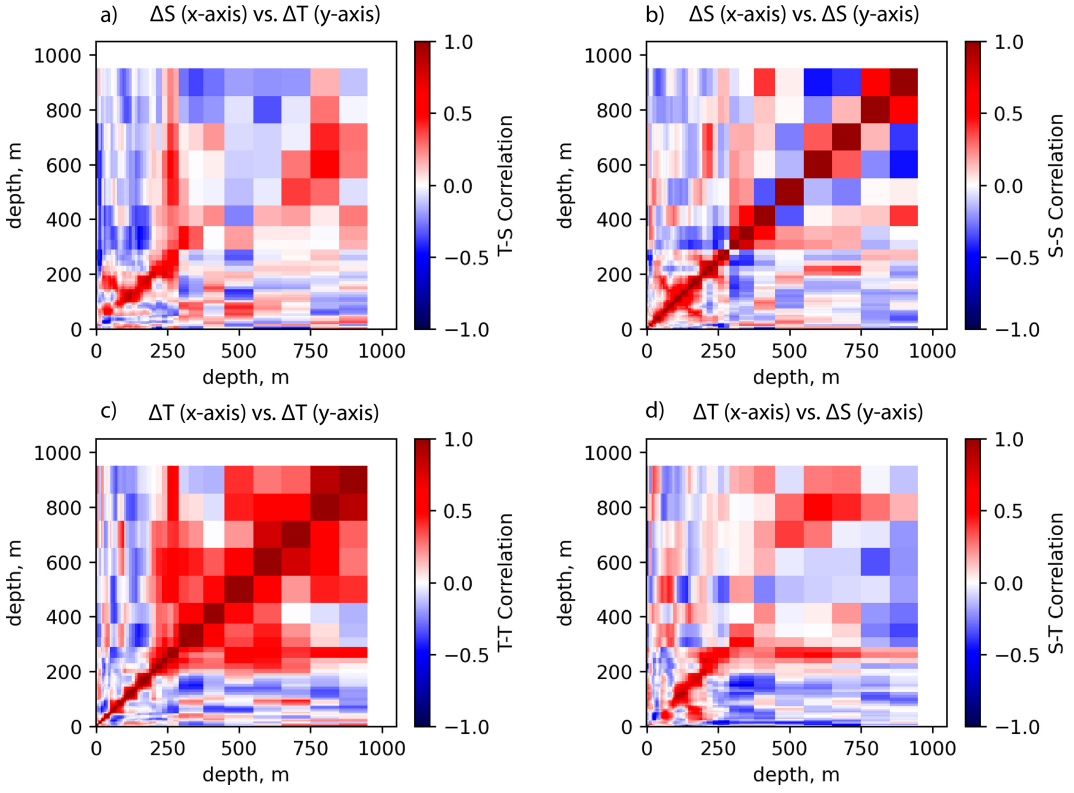

FIG. A1. The vertical gradient [see Eq. (A6)] correlations for ΔT and ΔS at 70°N, 3°E. The autocorrelations for ΔT and ΔS are along the diagonal in (b) and (c). The off-diagonal correlations for ΔS with ΔT and ΔT with ΔS are in (a) and (d). Since the correlations go from 0 to 1000 m, the ? and ? axes cover the same depths. The block structure indicates there are 47 depth levels in the upper 1000 m, where the block indicates depth bins that get larger with depth. The vertical gradient correlation $\mathbf{C}$ components (a) $\mathbf{C}^{(d)(T-S)}$, (b) $\mathbf{C}^{(d)(S-S)}$, (c) $\mathbf{C}^{(d)(T-T)}$, and (d) $\mathbf{C}^{(d)(S-T)}$ for the location 70°N, 0° in the high North Atlantic.

From Eq. (A3), we see that the solution is solved from the depth level just below the MLD. Thus, there is a procedure for translating the SST in Eq. (A16), down to the depth level k_{mld} (Helber et al. 2013). The last term in Eq. (A1) is the constraint of the synthetic profiles to the observed sea surface height anomaly $\delta\tilde{h}$. This input value differs from the variable in Eq. (A1), $\delta\tilde{h}^{(\mathrm{clim})}$, such that

$$\delta\tilde{h}^{(\mathrm{clim})} = \delta\tilde{h} + h^{(\mathrm{annual})} - h^{(\mathrm{clim})}, \tag{A17}$$

where $h^{(\mathrm{annual})}$ is the steric height referenced to 1000 m, as computed from historical in situ profile observations. The last variable, $h^{(\mathrm{clim})}$, is the climatological monthly steric height referenced to 1000 m, as computed from historical in situ profile observations. Thus, $\delta\tilde{h}^{(\mathrm{clim})}$ is the deviation of the observed

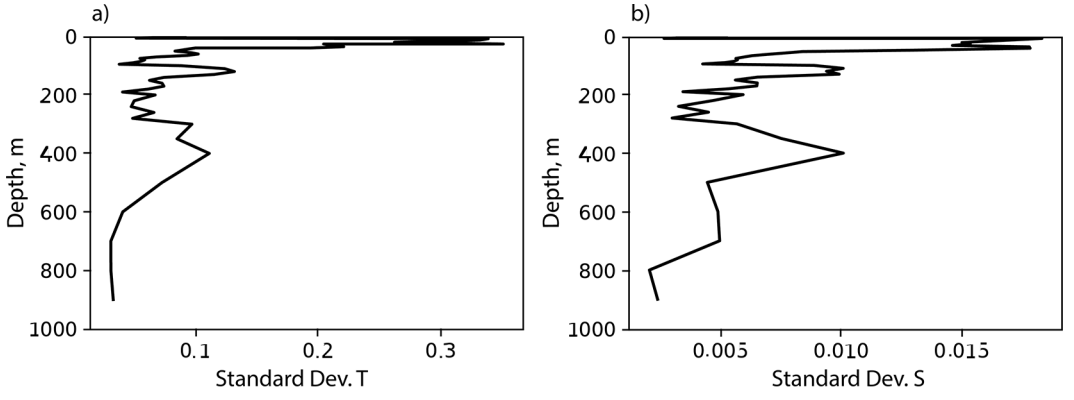

FIG. A2. The vertical gradient standard deviation profile for T and S for June at 70°N, 3°E, corresponding with the correlations shown in Fig. A1.

sea surface height from the climatological steric height. Because the input observed sea surface height anomaly operationally will come from satellite altimetry observations, this anomaly is relative to a long-term altimetry mean. Thus, our approach assumes that the actual full sea surface height is approximately

$$\tilde{h} \cong \delta\tilde{h} + h^{(\text{annual})}. \tag{A18}$$

The notation, $\mathbf{L}\delta\mathbf{x}^{(\text{clim})}$, in the last term of Eq. (A1) represents an application of the linearized operator $\mathbf{L}$, which computes the anomaly of the synthetic steric height referenced to 1000 m relative to climatology for the month. Thus, $\mathbf{L}\delta\mathbf{x}^{(\text{clim})} - \delta\tilde{h}^{(\text{clim})}$ is the difference of the synthetic minus the observed anomaly from climatology. The cost function form of this term [last term in Eq. (1)] includes $R^{(\text{SSHA})}$, which is the estimated error variance for $\delta\tilde{h}$.

Note, the solution obtained by minimizing the cost function [Eq. (A1)] are synthetic values of T and S that represent an estimate for the time and location of the observed surface values. Thus, the steric height of the resulting synthetic will match $\delta\tilde{h} + h^{(\text{annual})}$ from Eq. (A17) most closely.

REFERENCES

Bauer, R. A., 1985: *Functional Description Master Oceanographic Observation Data Set (MOODS)*. Compass Systems, Inc., 67 pp.

Bleck, R., 2002: An oceanic general circulation model framed in hybrid isopycnic-Cartesian coordinates. *Ocean Modell.*, **4**, 55–88, https://doi.org/10.1016/S1463-5003(01)00012-9.

Carnes, M., R. W. Helber, C. N. Barron, and J. M. Dastugue, 2010: Valication Test Report for GDEM4. NRL Memo. Rep. NRL/MR/7330–10-9271, 65 pp., https://apps.dtic.mil/sti/pdfs/ADA530343.pdf.

Chassignet, E. P., L. T. Smith, G. R. Halliwell, and R. Bleck, 2003: North Atlantic simulations with the Hybrid Coordinate Ocean Model (HYCOM): Impact of the vertical coordinate choice, reference pressure, and thermobaricity. *J. Phys. Oceanogr.*, **33**, 2504–2526, https://doi.org/10.1175/1520-0485(2003)033<2504:NASWTH>2.0.CO;2.

——, and Coauthors, 2009: US GODAE: Global ocean prediction with the HYbrid Coordinate Ocean Model (HYCOM). *Oceanography*, **22** (2), 64–75, https://doi.org/10.5670/oceanog.2009.39.

——, and Coauthors, 2020: Impact of horizontal resolution on global ocean–sea ice model simulations based on the experimental protocols of the Ocean Model Intercomparison Project phase 2 (OMIP-2). *Geosci. Model Dev.*, **13**, 4595–4637, https://doi.org/10.5194/gmd-13-4595-2020.

Fine, E. C., J. L. McClean, D. P. Ivanova, A. P. Craig, A. J. Wallcraft, E. P. Chassignet, and E. C. Hunke, 2023: Arctic ice-ocean interactions in an 8-to-2 kilometer resolution global model. *Ocean Modell.*, **184**, 102228, https://doi.org/10.1016/j.ocemod.2023.102228.

Hecht, M., and Coauthors, 2019: E3SMv0-HiLAT: A modified climate system model targeted for the study of high-latitude processes. *J. Adv. Model. Earth Syst.*, **11**, 2814–2843, https://doi.org/10.1029/2018MS001524.

Helber, R. W., T. L. Townsend, C. N. Barron, J. M. Dastugue, and M. R. Carnes, 2013: Validation Test Report for the Improved Synthetic Ocean Profile (ISOP) System, Part I: Synthetic Profile Methods and Algorithm. NRL Memo. Rep. NRL/MR/7320–13-9364, 128 pp., https://apps.dtic.mil/sti/pdfs/ADA585251.pdf.

——, and Coauthors, 2023: Ocean drifter velocity data assimilation, Part 1: Formulation and diagnostic results. *Ocean Modell.*, **183**, 102195, https://doi.org/10.1016/j.ocemod.2023.102195.

Hogan, T. F., and Coauthors, 2014: The Navy Global Environmental Model. *Oceanography*, **27** (3), 116–125, https://doi.org/10.5670/oceanog.2014.73.

Hunke, E. C., W. H. Lipscomb, A. K. Turner, N. Jeffery, and S. Elliot, 2015: CICE: The Los Alamos Sea Ice Model Documentation and Software User's Manual Version 5.1. LANL Doc. LA-CC-06-012, 116 pp., https://zenodo.org/records/19207490.

McDougall, T. J., and O. A. Krzysik, 2015: Spiciness. *J. Mar. Res.*, **73**, 141–152, https://doi.org/10.1357/002224015816665589.

Metzger, E. J., and Coauthors, 2014: US Navy operational global ocean and Arctic ice prediction systems. *Oceanography*, **27** (3), 32–43, https://doi.org/10.5670/oceanog.2014.66.

——, and Coauthors, 2020: Validation Test Report for the Global Ocean Forecast System 3.5—1/25° HYCOM/CICE with Tides. NRL Memo. Rep. NRL/MR/7323–19-9975, 73 pp., https://apps.dtic.mil/sti/pdfs/AD1113389.pdf.

Miyazawa, Y., and Coauthors, 2009: Water mass variability in the western North Pacific detected in a 15-year eddy resolving ocean reanalysis. *J. Oceanogr.*, **65**, 737–756, https://doi.org/10.1007/s10872-009-0063-3.

Oke, P. R., G. B. Brassington, D. A. Griffin, and A. Schiller, 2008: The Bluelink ocean data assimilation system (BODAS). *Ocean Modell.*, **21**, 46–70, https://doi.org/10.1016/j.ocemod.2007.11.002.

Raj, R. P., I. Halo, S. Chatterjee, T. Belonenko, M. Bakhoday-Paskyabi, I. Bashmachnikov, A. Fedorov, and J. Xie, 2020: Interaction between mesoscale eddies and the gyre circulation in the Lofoten Basin. *J. Geophys. Res. Oceans*, **125**, e2020JC016102, https://doi.org/10.1029/2020JC016102.

Strang, G., 2006: *Linear Algebra and Its Applications*. 4th ed. Thomson, Brooks/Cole, 487 pp.

Teague, W. J., E. J. Molinelli, and M. J. Carron, 1987: A new system for management of the "Master Oceanographic Observation Data Set" (MOODS). *EOS, Trans. Amer. Geophys. Union*, **68**, 553–559, https://doi.org/10.1029/EO068i022p00553-02.

Thoppil, P. G., and Coauthors, 2021: Ensemble forecasting greatly expands the prediction horizon for ocean mesoscale variability. *Commun. Earth Environ.*, **2**, 89, https://doi.org/10.1038/s43247-021-00151-5.

Tsujino, H., and Coauthors, 2018: JRA-55 based surface dataset for driving ocean–sea-ice models (JRA55-do). *Ocean Modell.*, **130**, 79–139, https://doi.org/10.1016/j.ocemod.2018.07.002.

Wijffels, S. E., G. Gebbie, and P. E. Robbins, 2024: Resolving the ubiquitous small-scale semipermanent features of the general ocean circulation: A multiplatform observational approach. *J. Phys. Oceanogr.*, **54**, 2503–2521, https://doi.org/10.1175/JPO-D-23-0225.1.